

MEMO - V1

Study of Correlations and Production between pairs of Charm-Anticharm particles

César Castromonte F.
Centro Brasileiro de Pesquisas Físicas
Rio de Janeiro, Brazil

1 Introduction

First order QCD predictions together with the standard Lund Model fragmentation model reproduce most of the kinematical properties of the charmed particles. However, many other aspects remain elusive and cannot be described without including a variety of non-perturbative effects.

For the charm quark, first order QCD predicts only to a back-to-back production of the c and \bar{c} quarks in the transverse plane to the beam direction, therefore, correlations between pairs of particles charm-anticharm are expected to be sensitive to non-perturbative effects and higher-order QCD corrections.

Particularly, charm-pair correlations between D and \bar{D} mesons have been widely studied, both theoretical [1–8], as well as experimentally in hadroproduction [9–14] and photoproduction [15–17].

In this memo we show the results about the study of charm-pair correlations between the particles D^\pm , D^0 , \bar{D}^0 , D_s and Λ_c (the last three one particles never included in previous photoproduction results) photoproduced by the E831/FOCUS experiment.

We present our results by comparing FOCUS data distributions to predictions from PYTHIA Monte Carlo generator [18] based on the Lund model, which includes non-perturbative effects that have been shown to be important in charm production. The procedures of selection and reconstruction of charm-pair candidates by using a candidate-driven algorithm to collect a large sample of fully reconstructed charmed particles are also described.

As an addition, we compare the charm-pair/anticharm-pair reconstructed yield ratios between data and Monte Carlo.

2 Reconstruction and Selection of Charm-pair events

The data used is from 65 DST files ... , where we use the Double-Dee skim from the EZDEE [19] block in order to find the pair candidates we are interested. In this EZDEE block each particle has an identification number which indicates the decay mode.

In Table 1 we can see the decay modes considered for this analysis (for each decay mode we are also considering its charged-conjugate mode).

Table 1: EZDEE particle ID's and the Decay modes.

EZDEE ID	Particle	Decay mode
1	D^+	$K^-\pi^+\pi^+$
2	D^0	$K^-\pi^+$
3	D^0	$K^-\pi^+\pi^-\pi^+$
5	D_s^+	$K^+K^-\pi^+$
37	Λ_c^+	$pK^-\pi^+$

2.1 The Reconstruction Procedure

The reconstruction algorithm considered all combinations of two, three and four charged tracks in order to find a combination that could be associated with the decay of a single charm particle¹. For each track the algorithm considers all possible combinations of charged K or π assignments such that the assignments are consistent with the decay of a charged or neutral charm particles. A particular combination of tracks and the associated particle assignments is referred to as a charm particle candidate. By using the measured track momenta we calculate the invariant mass of each charm particle which is required to fall within wide ranges:

$$\begin{aligned} D^+, D^0, D_s &\rightarrow 1.6 < m_D < 2.4 \text{ GeV}/c^2 \\ \Lambda_c &\rightarrow 1.89 < m_{\Lambda_c} < 2.69 \text{ GeV}/c^2 \end{aligned}$$

To select charm-pair particles we split the candidates in two sets, **A** and **B**, according to the topology of their decay modes. In set **A** we group the particles D^+ and D^0 , containing a kaon with the same charge (K^-), and in set **B** we group the particles D_s^+ and Λ_c^+ , containing a pion with the same charge (π^+). In Table 2 we show the criteria used.

Table 2: Selection criteria used to select charm-pair candidates.

Pair combs.	Charges
$A_1\bar{A}_2$	$K_1 \neq K_2$
$A_1\bar{B}_2$ ($B_1\bar{A}_2$)	$K_1 = \pi_2$ ($\pi_1 = K_2$)
$B_1\bar{B}_2$	$\pi_1 \neq \pi_2$

The second stage of the process is to find a pair of charm particle decay vertices that can be associated with a primary interaction vertex, and to find all other tracks in the event that can be associated with the primary vertex. This process starts by performing a vertex fit for each charm particle in the pair candidate and requiring

¹From now on, any reference to "charm particle" implies both the charm and anticharm particle.

that the tracks of each one of them form a vertex with confidence level greater than 1%. The charm pair candidates that satisfy the confidence level cut are subjected to two additional vertex cuts. The first requires that the momentum vectors of the two candidates intersect with a confidence level greater than 1%. The second cut reject pairs of charm particle candidates for which the reconstructed daughter tracks for both charm particles form a single vertex with confidence level greater than 1%. This rejects background events in which tracks for both candidates all come from a common vertex. Finally, the two charm particle candidates are treated as *seed tracks* to find the primary vertex. Using this two *seeds* as well as combinations of all other tracks in the event we perform a vertex fit, where as many tracks as possible are added as long as the confidence level is greater than 1%.

The pair candidates which survive the vertex reconstruction are subjected to particle-identification cuts, which are based on measurements from three multicell threshold Čerenkov counters. The Čerenkov algorithm [20] makes use of the on/off status of the cells to construct a likelihood for each one of the four hypothesis (electron, pion, kaon, proton) considered for each charged track. The algorithm produces a χ^2 -like variable $W_\alpha = -2\ln(\mathcal{L}_\alpha)$, where \mathcal{L} is the likelihood and α is the index used to represent each hypothesis. We identify particles by comparing these variables.

For the charged tracks of each charm particle we have:

$$\begin{aligned} W_\pi - W_K &> 1 && \text{(kaon)} \\ W_\pi - W_p &> 1 && \text{(proton)} \\ W_{\min} - W_\pi &> -5 && \text{(pion)} \end{aligned}$$

where W_{\min} is the W_α with the smallest value.

After applying particle-identification cuts, we impose cuts based on the significance of detachment (L/σ_L) between each charm particle candidate and the primary vertex. L is the distance between the charm particle and the primary vertex, and σ_L its associated error. The values for this cut depends of the decay mode, whether the charm particle decay vertex is located between target elements (out of material, OoM) or in target material, and whether a D^0 can be associated with a D^* decay. In Table 3 we can see these values.

Table 3: L/σ_L cut values

Decay mode	L/σ_L cut
$D^0 \rightarrow K^- \pi^+$	$L/\sigma_L > 1$
$D^+ \rightarrow K^- \pi^+ \pi^+$ $D_s^+ \rightarrow K^+ K^- \pi^+$ $\Lambda_c^+ \rightarrow p K^- \pi^+$	If OoM $< 0.5 \Rightarrow L/\sigma_L > 5$, otherwise $L/\sigma_L > 1$
$D^0 \rightarrow K^- \pi^+ \pi^- \pi^+$	If $\Delta M(D^* - D^0) > 0.003$ and OoM $< 0.5 \Rightarrow L/\sigma_L > 5$, otherwise $L/\sigma_L > 1$

2.1.1 The D_s Sample

In order to select the D_s candidates we use two resonant decay modes:

$$\begin{aligned} D_s^+ &\rightarrow \phi(1020)\pi^+, & \phi(1020) &\rightarrow K^+K^- \\ D_s^+ &\rightarrow \bar{K}^{*0}(892)K^+, & \bar{K}^{*0}(892) &\rightarrow K^-\pi^+ \end{aligned}$$

These two modes have much better signal-to-background ratio than inclusive $D_s^+ \rightarrow K^+K^-\pi^+$ decays. The $\phi(1020)\pi^+$ ($\bar{K}^{*0}(892)K^+$) decay mode candidates are required to have K^+K^- ($K^-\pi^+$) masses within two sigma of the nominal $\phi(1020)$ ($\bar{K}^{*0}(892)$) mass (Fig. 1). Other magnitude used to select the D_s candidates is the cosine of the angle ($\text{Cos}\theta$) between K^+ and the K^- (π^+) in the $\phi(1020)$ ($\bar{K}^{*0}(892)$) center-of-mass frame. It was required a cut of $|\text{Cos}\theta| > 0.3$ (0.6) for the $\phi(1020)\pi^+$ ($\bar{K}^{*0}(892)K^+$) decay modes respectively, as shown in Fig. 2. For the $\bar{K}^{*0}(892)K^+$ decay mode, the K^+K^- invariant mass must not be within two sigma of the $\phi(1020)$ mass to ensure statistically independent samples in the two decay modes.

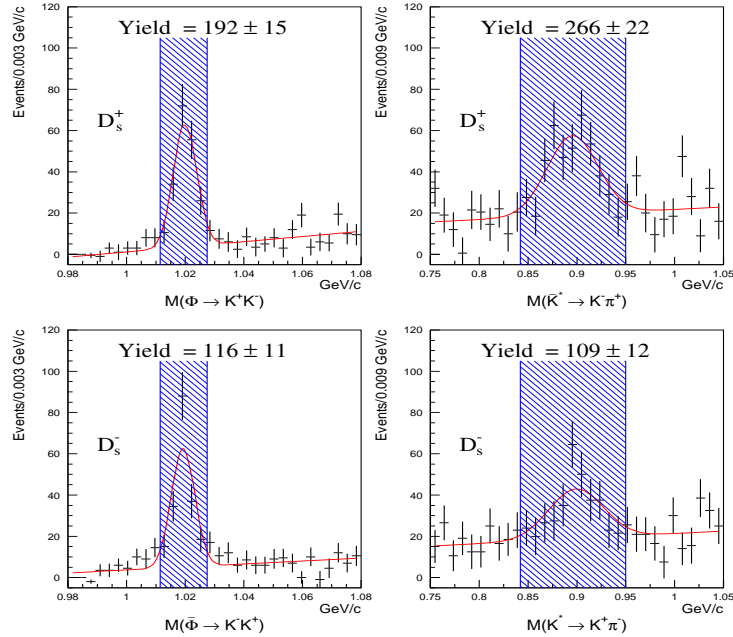


Figure 1: $\phi(1020)$ and $\bar{K}^{*0}(892)$ invariant mass distributions for particles (upper plots) and antiparticles (lower plots).

2.2 The Final Charm-pair Sample

After applied all the aforementioned selection and reconstruction criteria we get the sample of charm-pairs we use in the present analysis. This sample consists of the

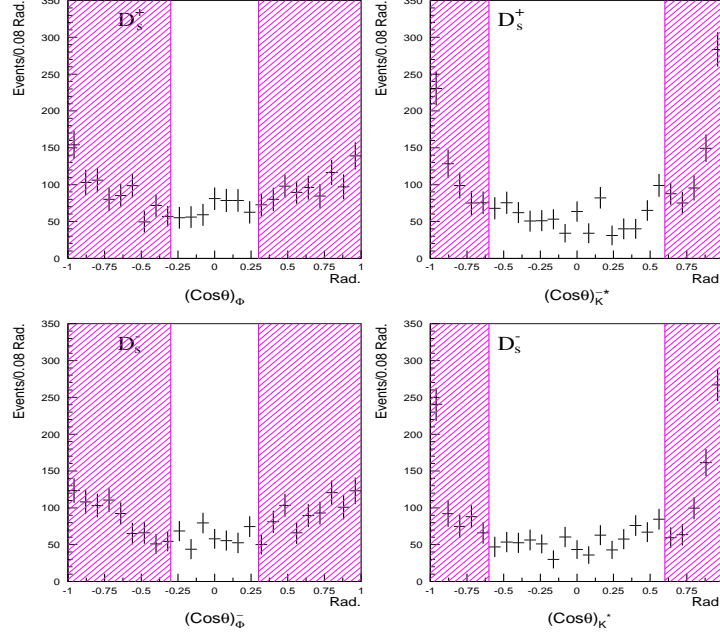


Figure 2

reconstructed charm-pairs: D^+D^- , $D^+\bar{D}^0$, D^0D^- , $D^0\bar{D}^0$, $D^+D_s^-$, $D_s^+D^-$, $D^0D_s^-$, $D_s^+\bar{D}^0$, $D^+\Lambda_c^-$, $\Lambda_c^+D^-$, $D^0\Lambda_c^-$, $\Lambda_c^+\bar{D}^0$, $D_s^+D_s^-$, $D_s^+\Lambda_c^-$, $\Lambda_c^+D_s^-$ and $\Lambda_c^+\Lambda_c^-$.

2.2.1 Bi-dimensional Normalized Invariant Mass Distributions of the Charm-pairs

In Figs. [3-7] we show the 2-dimensional normalized invariant mass² distributions (charm vs. anticharm particles) for several charm-pair combinations.

The $D_s^+D_s^-$, $D_s^+\Lambda_c^-$, $D_s^-\Lambda_c^+$ and $\Lambda_c^+\Lambda_c^-$ sub-samples (Fig. 7) were not used in the analysis due their poor statistics or too much background ($\Lambda_c^+\Lambda_c^-$).

On the other hand, Fig. 8 shows the scatter plot of the 2-dimensional normalized invariant mass for all the charm-pair combinations.

Three types of charm-pairs events are evident in this scatter plot. Combinatoric background consisting of pairs of fakes charm-anticharm particles are spread over the entire plot. Pairs containing one real charm (anticharm) and one fake anticharm (charm) particles appear as vertical and horizontal bands (called charm and anticharm ridge events respectively). In the center of the plot, we can see an enhancement due to the crossing of the two bands and due to real charm-pairs (signal region).

²The normalized mass is defined as: $M_n = \frac{M - M_{PDG}}{\sigma_M}$, where M is the measured mass, M_{PDG} is the PDG nominal mass, and σ_M is the associated error of the measurement.

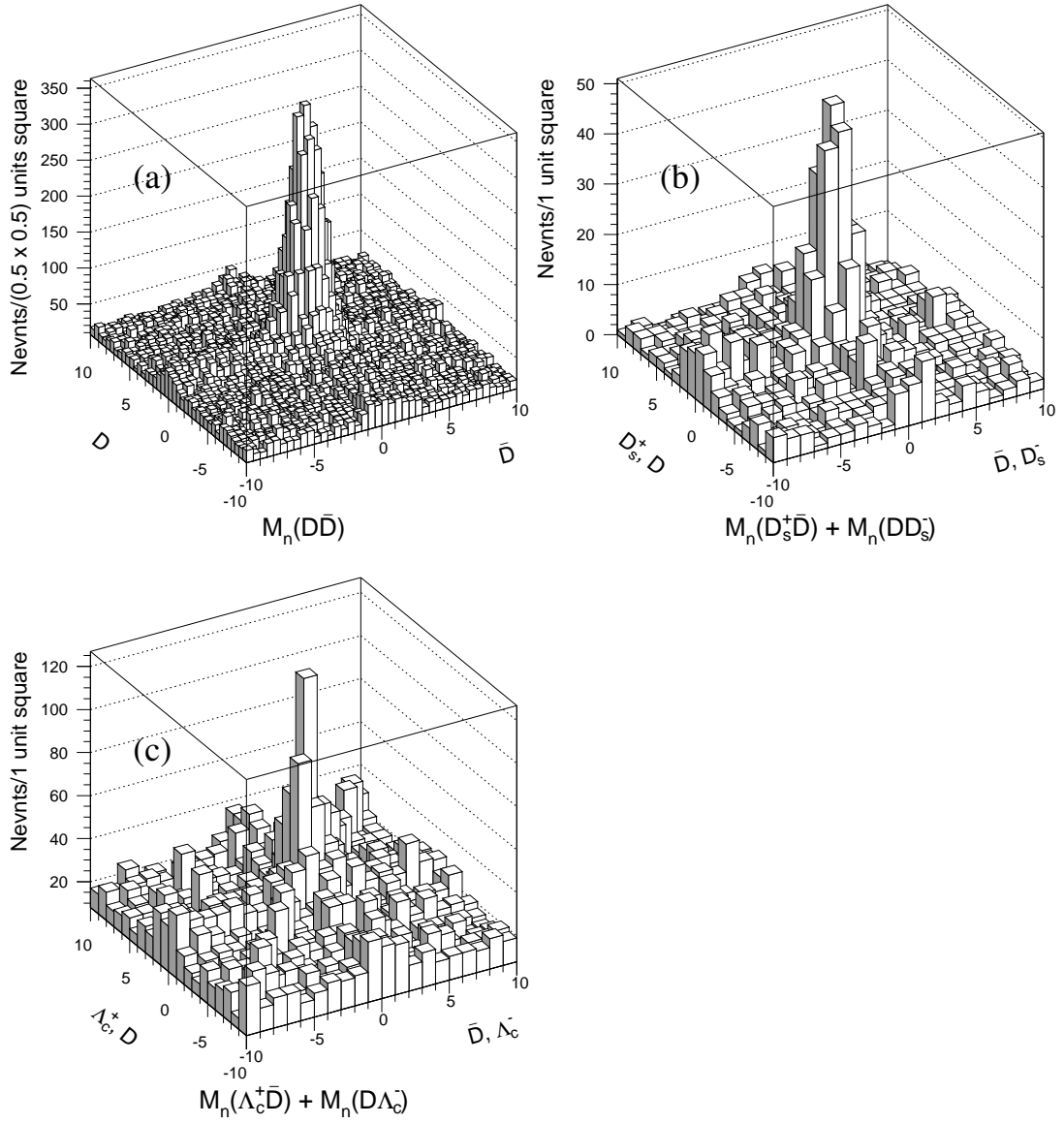


Figure 3: Charm-anticharm normalized invariant mass particle distributions for the pairs (a) $D\bar{D}$, (b) $D_s^+\bar{D}$ (+ charge conj.) and (c) $\Lambda_c^+\bar{D}$ (+ charge conj.).

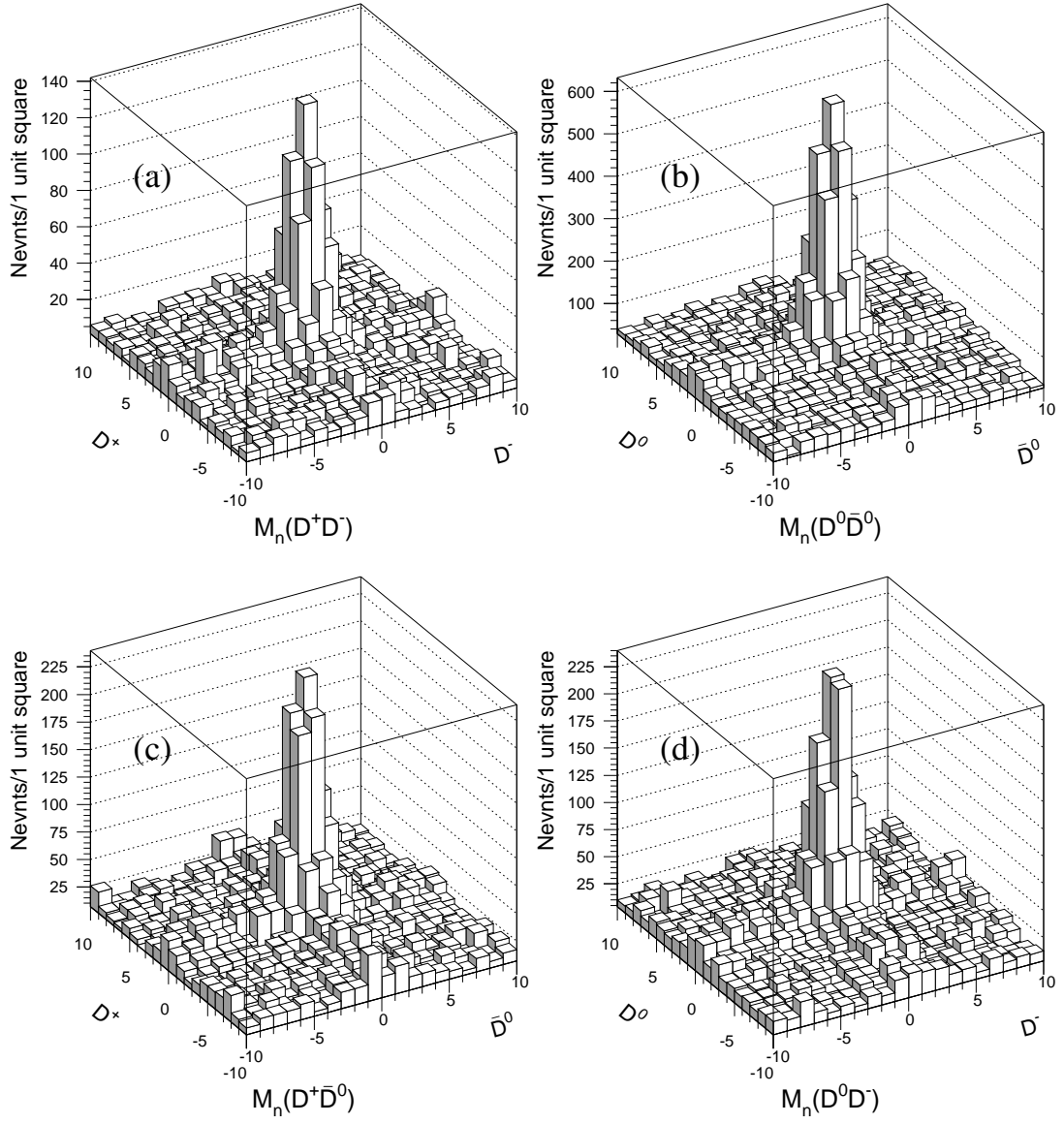


Figure 4: Charm-anticharm normalized invariant mass particle distributions for (a) D^+D^- , (b) $D^0\bar{D}^0$, (c) $D^+\bar{D}^0$ and (d) D^0D^- pairs.

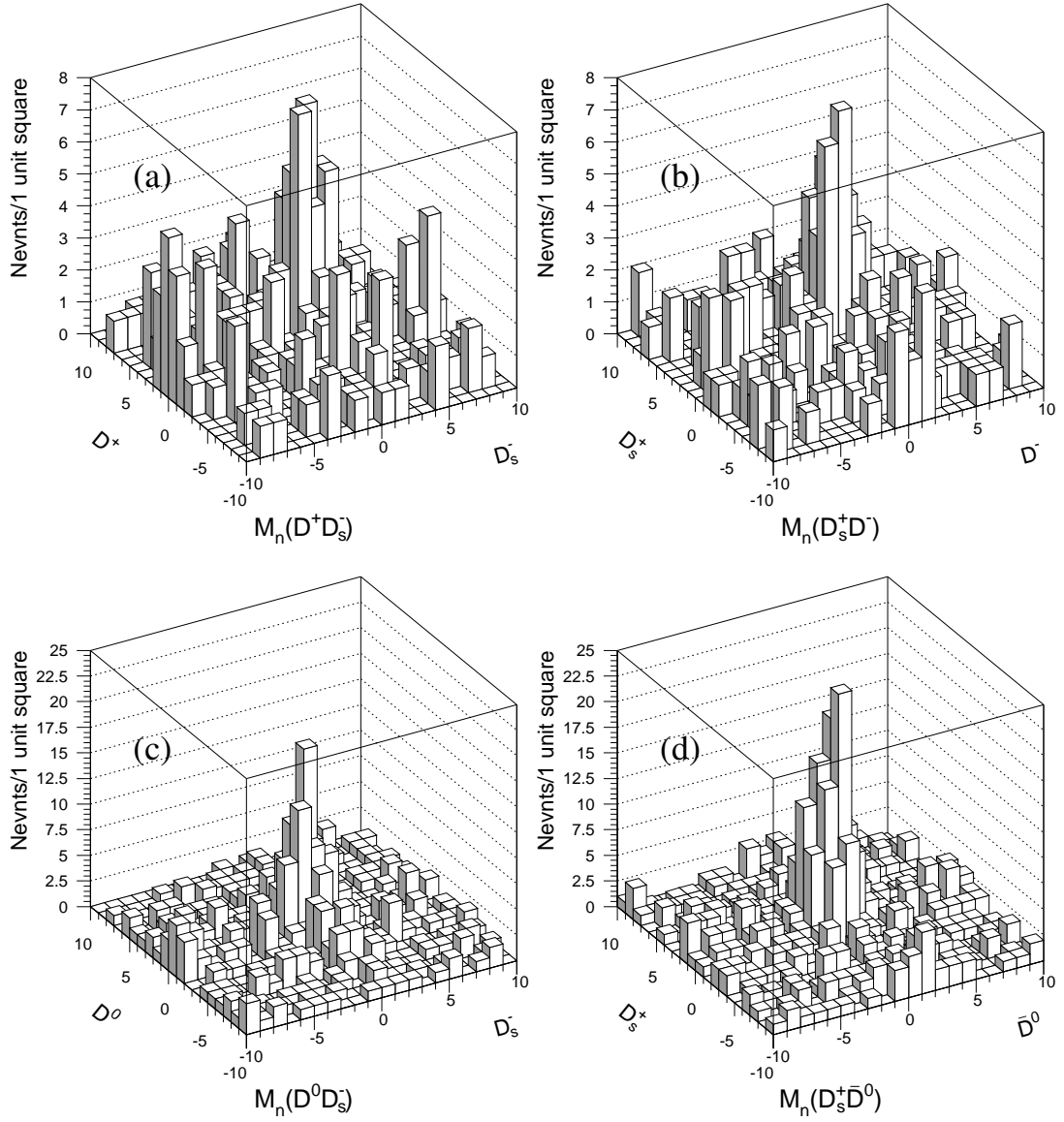


Figure 5: Charm-anticharm normalized invariant mass particle distributions for (a) $D^+D_s^-$, (b) $D_s^+D^-$, (c) $D^0D_s^-$ and (d) $D_s^+D^0$ pairs.

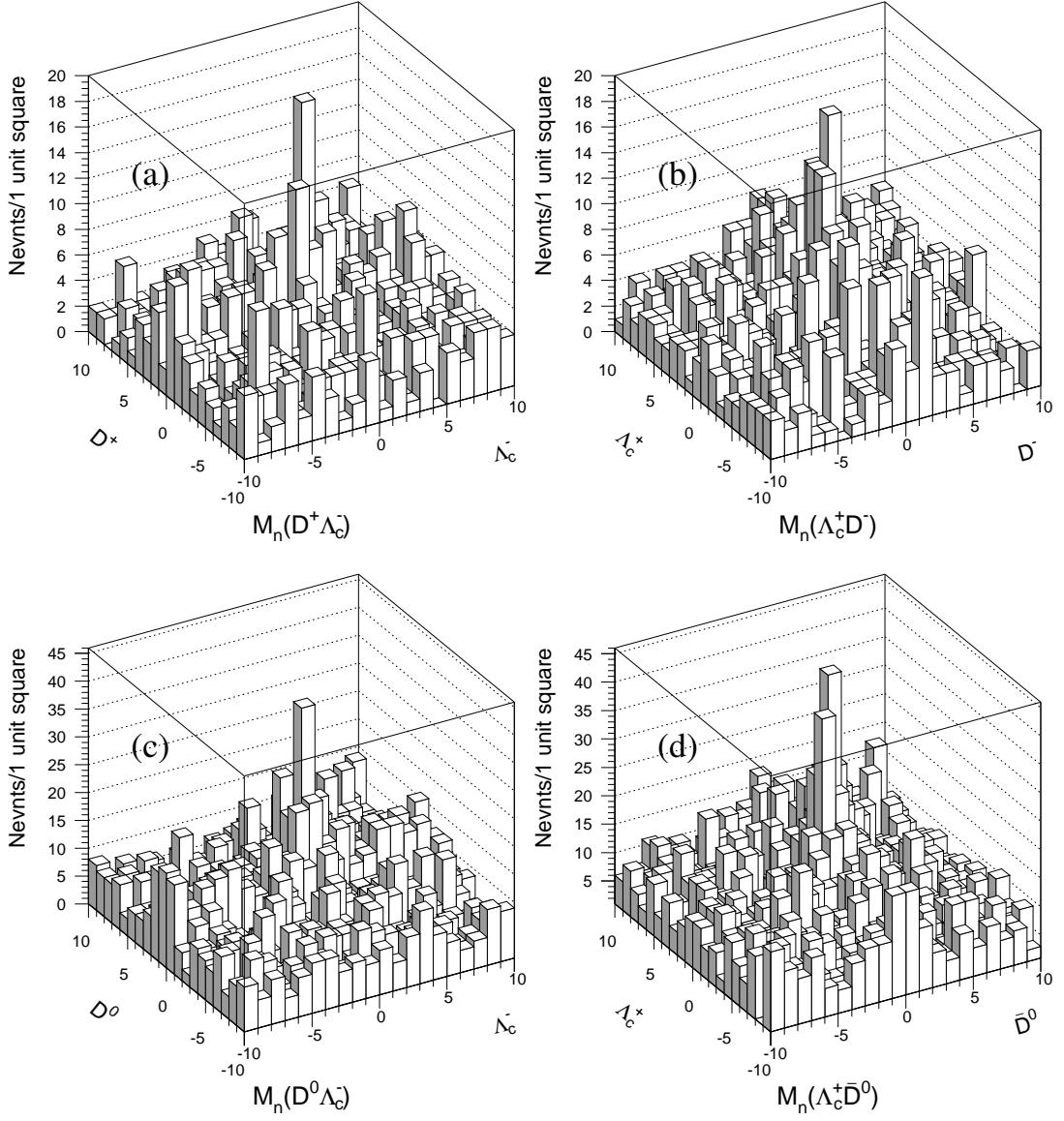


Figure 6: Charm-anticharm normalized invariant mass particle distributions for (a) $D^+\Lambda_c^-$, (b) $\Lambda_c^+D^-$, (c) $D^0\Lambda_c^-$ and (d) $\Lambda_c^+D^0$ pairs.

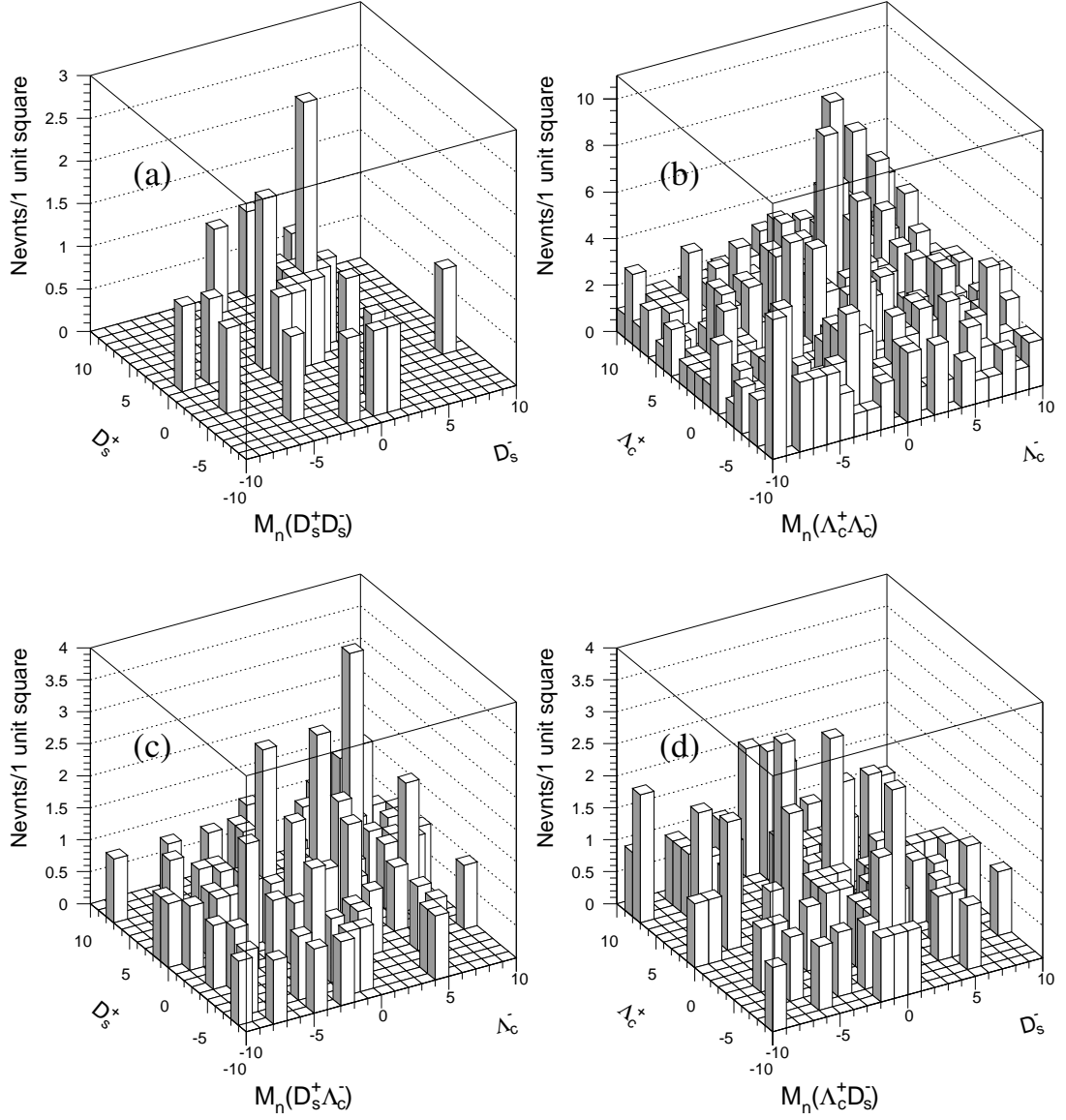


Figure 7: Charm-anticharm normalized invariant mass particle distributions for (a) $D_s^+ D_s^-$, (b) $\Lambda_c^+ \Lambda_c^-$, (c) $D_s^+ \Lambda_c^-$ and (d) $\Lambda_c^+ D_s^-$ pairs.

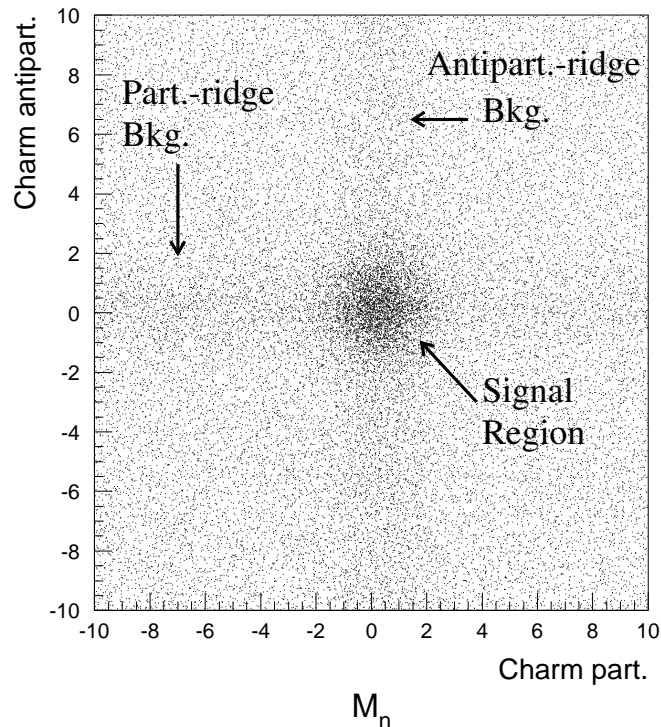


Figure 8: Scatter plot of normalized charm particle versus normalized anticharm particle mass for the final charm-pair FOCUS sample.

2.2.2 Invariant Mass Distributions

Figs. [9-10] show the sideband subtracted³ invariant mass for each particle considered in the analysis (D , D_s and Λ_c) according to its decay mode.

In Fig. 9, apart from the peak corresponding to the actual mass we can observe a peak appearing about 2.1 GeV/c in the $K\pi\pi$ and $K\pi\pi\pi$ decay mode mass distributions that could be associated with a false D^* . In the first decay mode, the false D^* comes from a misreconstruction of the D^+ mass: $D^{*\pm} \rightarrow D^0(K\pi)\pi^\pm$. In the second decay mode, the false D^* is probably produced by a no identification of a neutral particle (γ or π^0): $D^{*0} \rightarrow D^0\gamma$ or $(D^0\pi^0)$.

In Fig. 10 we show the sideband subtracted D_s^\pm distributions for the two resonant decay modes used. Besides the D_s^+ peak, we also observe a second peak about 1.87 GeV/c for the two decay modes. This peak corresponds to a false D^+ and is produced due a misidentification of one K by one π . Finally in Fig. 11 we show the

³This procedure requires the charm-like (anticharm-like) variable to be projected by selecting events in the anticharm (charm) signal region ($\pm 2\sigma$ from the center) with weight unit, and events with weight of $-\frac{1}{2}$ in the two anticharm (charm) $4-8\sigma$ sideband regions, in the 2-dimensional normalized invariant mass distributions. (See Fig. 12)

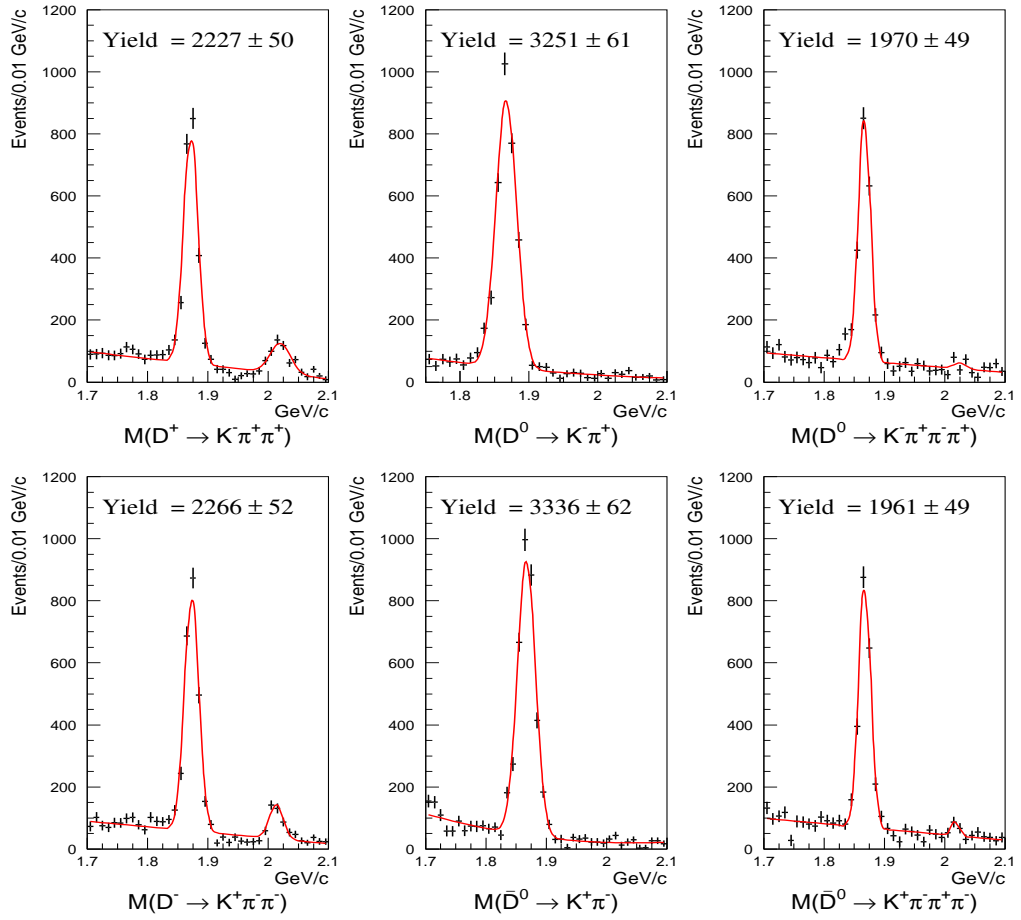


Figure 9: Fit to the sideband subtracted invariant mass distributions for data particles D^+ , D^0 , D^- and \bar{D}^0 .

Λ_c^\pm distributions.

To get the single-charm yields we performed a fit by using a Gaussian (or two, depending of the case) functions to model the signal(s), and a linear polynomial function to model the background. In Table 4 we summarize the yields obtained for each decay mode.

3 Data Analysis

In this section we describe the analysis procedures performed to study the charm-pair correlations as well as the calculate of the pair/antipair yield ratios for data and Monte Carlo.

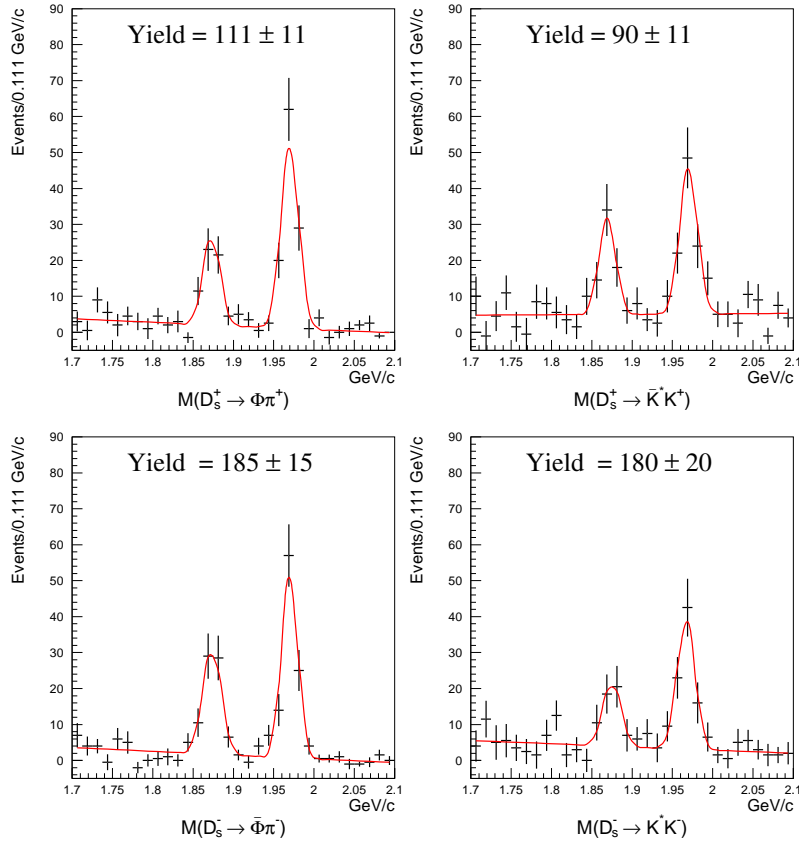


Figure 10: Fit to the sideband subtracted invariant mass distributions for data particles D_s^+ and D_s^- in the $\phi(1020)\pi^\pm$ and $K^*(892)^0K^\pm$ decay modes.

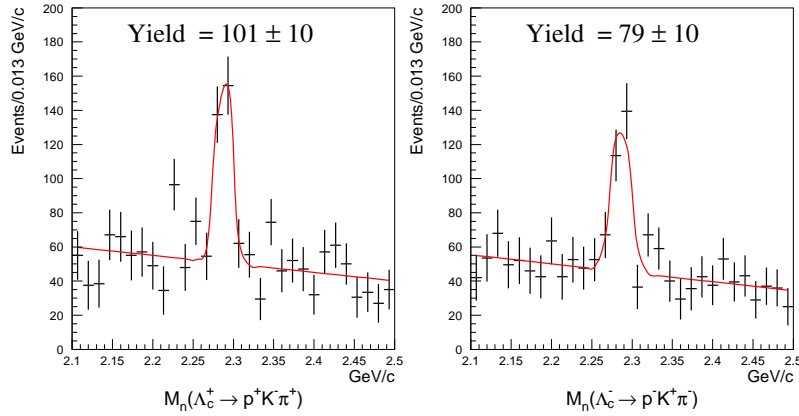


Figure 11: Fit to the sideband subtracted invariant mass distributions for data particles Λ_c^+ and Λ_c^- .

Table 4: Number of Signal events for each charm decay mode.

	Decay mode	Yield
Charm particles	$D^+ \rightarrow K^- \pi^+ \pi^+$	2227 ± 50
	$D^0 \rightarrow K^- \pi^+$	3251 ± 61
	$D^0 \rightarrow K^- \pi^+ \pi^- \pi^+$	1970 ± 49
	$D_s^+ \rightarrow \phi(1020) \pi^+$	111 ± 11
	$D_s^+ \rightarrow \bar{K}^*(892)^0 K^+$	90 ± 11
	$\Lambda_c^+ \rightarrow p^+ K^- \pi^+$	101 ± 10
Anticharm particles	$D^- \rightarrow K^+ \pi^- \pi^-$	2266 ± 52
	$\bar{D}^0 \rightarrow K^+ \pi^-$	3336 ± 62
	$\bar{D}^0 \rightarrow K^+ \pi^- \pi^+ \pi^-$	1961 ± 49
	$D_s^- \rightarrow \phi(1020) \pi^-$	185 ± 15
	$D_s^- \rightarrow K^*(892)^0 K^-$	180 ± 20
	$\Lambda_c^- \rightarrow p^- K^+ \pi^-$	79 ± 10

3.1 Determination of the Yields

In order to obtain physics distributions (e.g. charm-pair transversal momentum p_T , rapidity difference Δy , etc.), is necessary to have a method to determine the number of charm-pair signal events in each bin of a given physical variable.

Two methods were performed to do this: a binned method for background subtraction and a binned maximum-likelihood fit.

3.1.1 Binned background subtraction

A simpler way to count the number of charm-pairs in a determined sample is by performing a double background subtraction in the corresponding bi-dimensional normalized mass distribution.

To perform the double background subtraction we define four regions in the charm-anticharm normalized mass distributions according to their cross-hatching, as shown in Fig. 12:

- Region 1 (charm and anticharm candidates are $\pm 4-8\sigma$ away from the center), with N_1 events, contains mostly combinatoric background events;
- Region 2 ($\pm 2\sigma$ about the charm axis and $\pm 4-8\sigma$ about the anticharm axis), with N_2 events, contains both combinatoric background events and anticharm-ridge background events;
- Region 3 ($\pm 2\sigma$ about the anticharm axis and $\pm 4-8\sigma$ about the charm axis), with N_3 events, contains both combinatoric background events and charm-ridge background events;

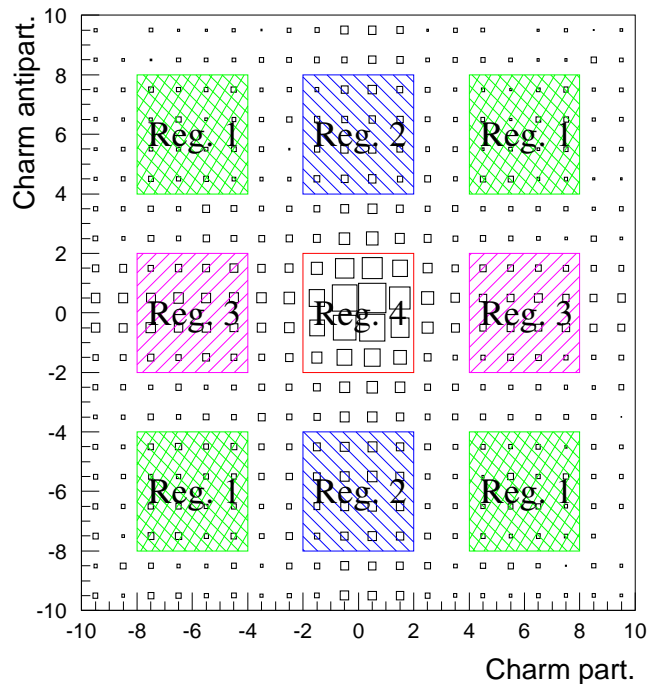


Figure 12: Scatter plot of normalized charm particle versus normalized anticharm particle mass for the final charm-pair FOCUS sample.

- Region 4 ($\pm 2\sigma$ about the center of the distribution), with N_4 events, contains signal events as well as the other three types of background events.

An estimate for the number of signal events is given by:

$$N_s = N_4 - 1/2(N_2 + N_3) + 1/4(N_1) \quad (1)$$

and the error in this estimate is given by:

$$\sigma_{N_s} = \sqrt{N_4 + (1/2)^2(N_2 + N_3) + (1/4)^2(N_1)} \quad (2)$$

As an example, for all the charm-pair combinations (Fig. 8) we have: $N_1 = 7452$ events, $N_2 + N_3 = 10972$ events and $N_4 = 10993$ events, and by using the equations 1 and 2 we obtain the number of charm-pairs in the signal region, $N_s = \mathbf{7500 \pm 136}$.

In Table 5 we summarize the charm-pair yields we get by using the counting method for several charm-pair sub-samples.

Table 5: Charm-pair number of events from the counting method.

Charm-pair	Yield
Total	7500 ± 136
D \bar{D}	6720 ± 125
D _s ⁺ \bar{D} + DD _s ⁻	300 ± 24
Λ _c ⁺ \bar{D} + DΛ _c ⁻	429 ± 47
D ⁺ \bar{D}^0	1303 ± 55
D ⁰ D ⁻	1301 ± 55
D ⁺ D _s ⁻	43 ± 10
D _s ⁺ D ⁻	44 ± 9
D ⁰ D _s ⁻	81 ± 13
D _s ⁺ \bar{D}^0	133 ± 15
D ⁺ Λ _c ⁻	47 ± 17
Λ _c ⁺ D ⁻	71 ± 18
D ⁰ Λ _c ⁻	137 ± 26
Λ _c ⁺ \bar{D}^0	175 ± 29
D ⁺ D ⁻	704 ± 38
D ⁰ \bar{D}^0	3412 ± 90

3.1.2 Binned Maximum Likelihood fit

Another (and more powerful) method to determine the number of charm-pairs in the signal region is by performing a maximum-likelihood fit.

To determine the number of signal events in each charm-pair sample considered, we perform a bi-dimensional fit over the charm-anticharm normalized mass distributions (Figs. 3-6). In general, the maximum likelihood method assumes we have N independent measurements of one or more quantities and that these quantities z_j are distributed according to some probability density function $\mathcal{F}(z_j|\vec{\theta})$, where $\vec{\theta}$ is a set of unknown parameters to be determined. To determine the set of values $\vec{\theta}$ that maximizes the joint probability for all events we have to solve numerically the set of equations:

$$\frac{\partial \ln \mathcal{L}(\vec{\theta})}{\partial \theta_j} = 0, \quad \text{where} \quad \mathcal{L}(\vec{\theta}) = \prod_{j=1}^N \mathcal{F}(z_j|\vec{\theta}) \quad (3)$$

In particular, for this analysis we use the *binned maximum likelihood* method. If we have a 2-dimensional histogram with $M \times N$ bins, where each bin has a constant bin-area s :

$$s = h_x \cdot h_y \quad ; \quad h_x \equiv \frac{(x_f - x_i)}{M} \\ h_y \equiv \frac{(y_f - y_i)}{N}$$

where x_f and x_i (y_f and y_i) are the upper and lower limits on X (Y) coordinate, then the fitted content of the bin $b(p, q)$ ($p = 1 \cdots M$, $q = 1 \cdots N$) will be:

$$f_{pq}(\vec{\theta}) = \int_{x_i+h_x \cdot (p-1)}^{x_i+h_x \cdot p} \int_{y_i+h_y \cdot (q-1)}^{y_i+h_y \cdot q} f(x, y|\vec{\theta}) dx dy \quad (4)$$

where $f(x, y|\vec{\theta})$ is the function which parametrizes the shape and height of the histogram (and for that reason does not need to be normalized).

If we assume a Poisson distribution for the number of events in each bin, n_{pq} , then the likelihood become:

$$\mathcal{L}(\alpha) = \prod_{i=1}^M \frac{(f_{pq})^{n_{pq}} e^{-f_{pq}}}{n_{pq}!} \quad (5)$$

It is always more convenient to work with the negative log-likelihood, so:

$$-\ln \mathcal{L}(\alpha) = - \sum_{i=1}^M (n_{pq} \ln f_{pq} - f_{pq} - \ln n_{pq}!) \quad (6)$$

In Eq. 6 we can drop the term $\sum_{i=1}^M \ln n_{pq}!$ because it is independent of α and does not alter the fit result. Ignoring this constant we obtain the function to minimize:

$$-\ln \mathcal{L}(\alpha) = - \sum_{i=1}^M (n_{pq} \ln f_{pq} - f_{pq}) \quad (7)$$

In order to construct the parametric function $f(x, y|\vec{\theta})$, we assume that: i) the normalized mass distribution of real charm and anticharm particle pairs is Gaussian, and ii) the normalized mass distribution for background of the pairs is linear, so the parametric function is:

$$f(x, y|\vec{\theta}) = N_S \cdot G_{2D}(x, y|\sigma_{x2D}, \sigma_{y2D}, \mu_x, \mu_y) + N_X \cdot G_{1D}(x|\sigma_x, \mu_x) + N_Y \cdot G_{1D}(y|\sigma_y, \mu_y) + N_B \cdot P_{2D}(x, y|b_x, b_y) \quad (8)$$

where G_{2D} , G_{1D} and P_{2D} are normalized sub-functions used to model:

$$\text{Signal events: } G_{2D}(x, y|\sigma_{x2D}, \sigma_{y2D}, \mu_x, \mu_y) = \frac{1}{2\pi \sigma_{x2D} \sigma_{y2D}} e^{-\frac{1}{2} \left[\left(\frac{x-\mu_x}{\sigma_{x2D}} \right)^2 + \left(\frac{y-\mu_y}{\sigma_{y2D}} \right)^2 \right]}$$

$$\text{Charm-ridge bkg. events: } G_{1D}(x|\sigma_x, \mu_x) = \frac{1}{\sqrt{2\pi} \sigma_x} e^{-\frac{1}{2} \left[\frac{x-\mu_x}{\sigma_x} \right]^2}$$

$$\text{Anticharm-ridge bkg. events: } G_{1D}(y|\sigma_y, \mu_y) = \frac{1}{\sqrt{2\pi} \sigma_y} e^{-\frac{1}{2} \left[\frac{y-\mu_y}{\sigma_y} \right]^2}$$

$$\text{Combin. events: } P_{2D}(x, y|b_x, b_y) = \frac{1}{(x_f-x_i)(y_f-y_i)} + b_x(x - m_x) + b_y(y - m_y)$$

The unknown parameters in the maximum likelihood fit are:

$$\boldsymbol{\alpha} = (N_S, N_B, N_x, N_y, \sigma_{x2D}, \sigma_{y2D}, \sigma_x, \sigma_y, \mu_x, \mu_y, b_x, b_y) \quad (9)$$

where:

N_S : number of signal events.

N_x : number of one real charm and one fake anticharm particle events.

N_y : number of one real anticharm and one fake charm particle events.

N_B : number of combinatorial background events.

$\sigma_{x2D}, \sigma_{y2D}$: X and Y Gaussian widths for the signal events.

σ_x, σ_y : Gaussian widths for the charm-ridge and anticharm-ridge background events.

μ_x, μ_y : mean masses for the charm and anticharm particles respectively.

b_x, b_y : the slopes of the combinatorial background for the charm and anticharm particles respectively.

To maximize the likelihood we use the function minimization and error analysis fortran package MINUIT [21]. Fig. 13 shows the shape of the function $f(x, y|\vec{\theta})$ that maximizes the likelihood function for the charm-pair mass distributions. The mass range used for all the fits in the analysis is $|M_n| < 10$.

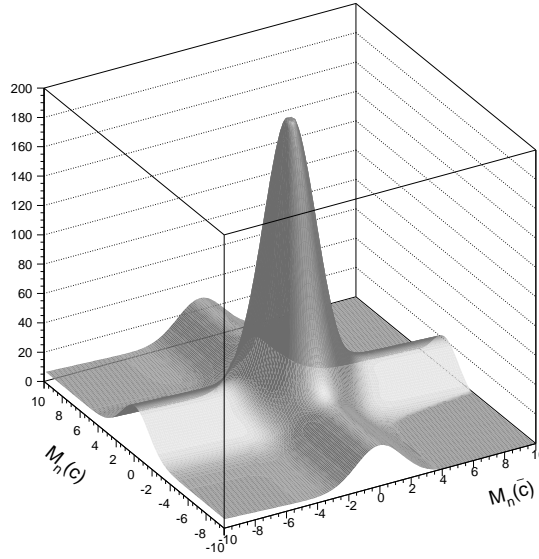


Figure 13: The function $f(M_n(c), M_n(\bar{c})|\vec{\theta})$ that maximizes the likelihood function for the charm-pairs samples shown in Figs. [3-6].

The total signal yield that we obtain by using this method is 8423 ± 144 events. In Table 6 we show a summary of the yields we get for the charm-pair samples. We can observe that the production of the Λ_c charm-pairs combinations is more than twice the production of the D_s charm-pair combinations. The $D_s^+ \Lambda_c^-$, $\Lambda_c^+ D_s^-$, $D_s^+ D_s^-$

and $\Lambda_c^+\Lambda_c^-$ distributions were not considered in the analysis due their poor statistics or too much background.

Table 6: Charm-pair number of events from the log-likelihood fit.

FOCUS Data	
Charm-pair	Yield
Total	8423 \pm 144
DD	7626 \pm 133
$D_s^+\bar{D} + DD_s^-$	317 \pm 24
$\Lambda_c^+\bar{D} + D\Lambda_c^-$	424 \pm 46
$D^+\bar{D}^0$	1463 \pm 61
D^0D^-	1509 \pm 59
$D^+D_s^-$	41 \pm 9
$D_s^+D^-$	49 \pm 9
$D^0D_s^-$	94 \pm 14
$D_s^+\bar{D}^0$	138 \pm 14
$D^+\Lambda_c^-$	44 \pm 10
$\Lambda_c^+D^-$	70 \pm 22
$D^0\Lambda_c^-$	131 \pm 27
$\Lambda_c^+\bar{D}^0$	197 \pm 22
D^+D^-	769 \pm 35
$D^0\bar{D}^0$	3938 \pm 98

From Tables 5 and 6 we can observe some differences between the number of events obtained by the two methods aforementioned. These differences come from the area considered in the count.

In the double background subtraction method (a simple counting method), a square area of $S_{xy} = \pm 2\sigma$ around the center of the mass distribution is selected in order to count the number of charm-pairs events. On the other hand, in the log-likelihood method we assume that the signal can be model by a 2-dimensional gaussian G_{2D} (see Eq. 8), so, if we integrate the bi-dimensional gaussian in the square area S_{xy} we should have the fraction of events given by the counting method.

So,

$$\begin{aligned}
Y_{count} &= Y_{log-like} \int_{S_{xy}} G_{2D}(x, y | \sigma_x, \sigma_y, \mu_x, \mu_y) \\
&= Y_{log-like} \left(\int_{\pm 2\sigma_x} G_{1D}(x | \sigma_x, \mu_x) \right) \left(\int_{\pm 2\sigma_y} G_{1D}(y | \sigma_y, \mu_y) \right) \\
&= Y_{log-like} (0.945) \times (0.945) \\
&\approx (0.89) Y_{log-like}
\end{aligned} \tag{10}$$

If we divide the total number of charm-pairs given by the two methods $Y_{count}(\approx 7500)/Y_{log-like}(\approx 8420)$, we've got ≈ 0.89 , which match very well with the expected fraction.

3.2 MC Sample

For the study of correlations and the pair/antipair ratios calculate between pairs of reconstructed charm particles, we compare the FOCUS data to predictions from a Monte Carlo simulation based on the Lund Model. The Monte Carlo consists of a PYTHIA 6.127 [18] generator and detector simulation algorithms for the FOCUS apparatus. The Monte Carlo generator produces charm events using the three-level photon-gluon fusion [22] process applied to beam photons and target nucleons, where a single topological graph (Fig. 14) is expected. The Lund string fragmentation model [23] is used to dress the quarks into hadrons, and an intrinsic transverse momentum of the incoming partons k_T is Gaussian distributed with a RMS width $\langle k_T^2 \rangle = (0.6 \text{ GeV}/c)^2$ ⁴.

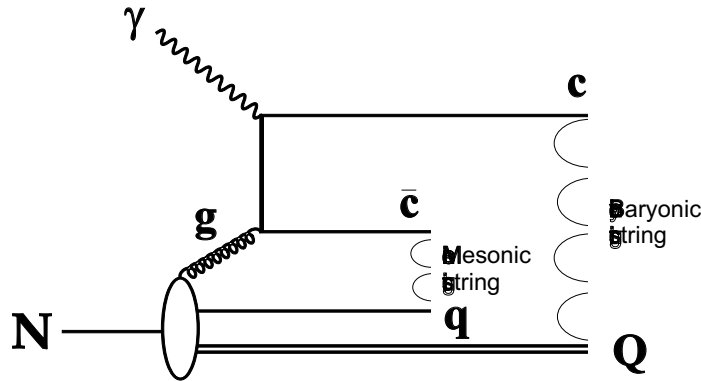


Figure 14: Tree-level photon-gluon fusion process.

As we are interested in performing the studies considering charm-pairs containing D_s and Λ_c particles, two sets of Monte Carlo were generated, the first set giving a better simulation for the production of D^+ 's and D^0 's (called **MCDD2**), whereas the second set were tuned to favor a better simulation for the production of D_s 's and Λ_c 's (called **MCDSL**). For each sample of Monte Carlo, 200 million of events were generated at the University of Colorado by Kevin Stenson. In Tables 7 and 8 we show the main common and specific parameters used to generate the two MC samples. In Appendix A we show how these parameters were set.

After passing the same cuts and selection criteria as the real data we obtain a reconstructed total MC sample of ≈ 55723 (MCDD2) and **60135** (MCDSL)

⁴The default value of $\langle k_T^2 \rangle$ for this PYTHIA version is $(0.44 \text{ GeV}/c)^2$.

Table 7: MC common settings

Parameter	Description	Used value	Default value
$E_{\text{cm}}(\text{min})$	The lowest c.m. energy for the event as a whole (in GeV).	3	10
m_Q	Charm quark mass (in GeV).	1.6	1.35
$\Delta\chi$	Range of allowed χ (nucleon momentum fraction) values for the bachelior quark inside the nucleon.	[0.,1.0001]	[0.,1.]
σ_{k_\perp}	Width of Gaussian primordial k_\perp distribution of the partons inside the nucleon, i.e. $\exp(-k_\perp^2/\sigma_{k_\perp}^2)k_\perp dk_\perp$, with $\langle k_\perp^2 \rangle = \sigma_{k_\perp}^2$	0.6	0.44
Cut-off in k_\perp	Upper cut-off for primordial k_\perp distribution for partons inside the nucleon.	3	2
$\frac{\mathcal{P}(\text{us})/\mathcal{P}(\text{ud})}{\mathcal{P}(\text{s})/\mathcal{P}(\text{d})}$	The extra suppression of strange di-quark production compared with the normal suppression of strange quarks.	0.25	0.4
Hadronizat. model	$f^{\text{Lund}}(z) \propto \frac{1}{z} z^{a_\alpha} \left(\frac{1-z}{z}\right)^{a_\beta} \exp\left(\frac{-bm_\perp^2}{z}\right)$	Lund	Lund
a, b	Parameters of the Lund fragmentation function (in GeV^{-2})	0.25, 0.7	0.3, 0.8

Table 8: MC specific model settings

Parameter	Description	MCDD2 value	MCDSL C value	Default value
$\mathcal{P}(\text{qq})/\mathcal{P}(\text{q})$	The suppression of s quark pair production in the field compared with u or d pair production.	0.3	0.5	0.1
$\mathcal{P}(\text{s})/\mathcal{P}(\text{u})$	The suppression of diquark-antidiquark pair production in the colour field, compared with quark-antiquark production.	0.3	0.25	0.3
$\frac{dN}{d\chi} \sim$	The energy fraction χ taken by the bachelior quark according to some dist. Here $c_{\text{min}} = 0.6 \text{ GeV}/E_{\text{cm}} \approx 2\langle m_Q \rangle/E_{\text{cm}}$.	$3(1-\chi)^2$	$\frac{(1-\chi)^2}{\sqrt{\chi^2+c_{\text{min}}^2}}$	$\frac{(1-\chi)^3}{\sqrt[4]{\chi^2+c_{\text{min}}^2}}$
a'	The amount to be added to the a parameter in the Lund flavour dependent symmetric fragmentation function for the diquarks production.	0.75	0.9	0.5

charm-pairs⁵, as shown in Fig. 15.

In Table 9 we show a summary of the reconstructed and generated yields for several charm-pair decays for the two Monte Carlo sets.

⁵The fit procedure to get the Monte Carlo yields is the same as used for real data (see section 3.1)

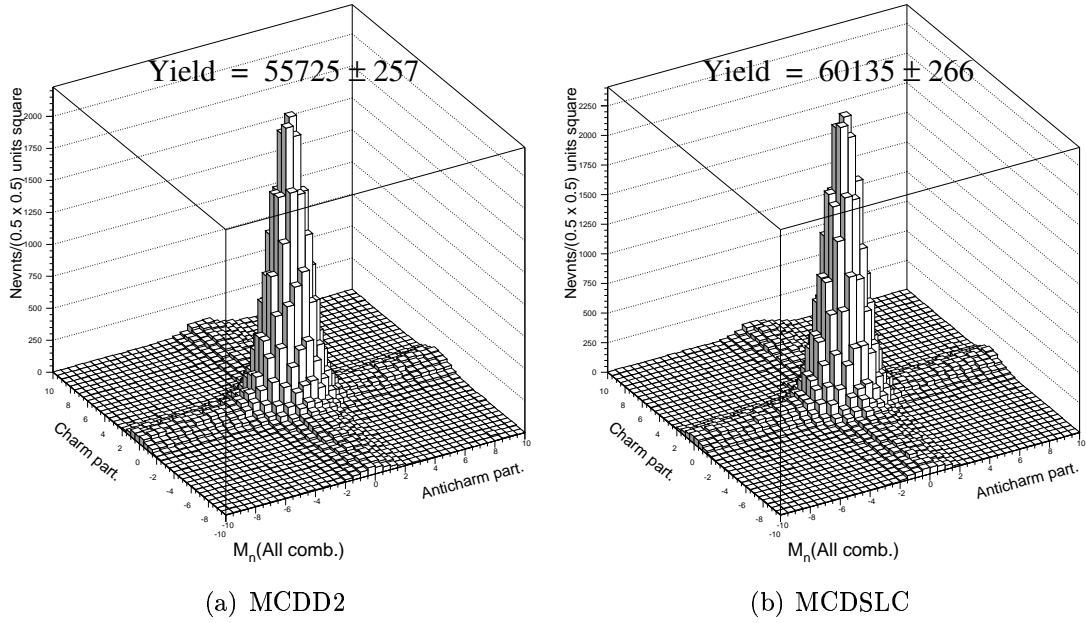


Figure 15: Total normalized invariant mass distributions for the two MC samples.

Table 9: Number of reconstructed and generated events for the two MC samples.

Charm-pair	MCDD2		MCDSL C	
	No. Event. Reconstructed	No. Event. Generated	No. Event. Reconstructed	No. Event. Generated
All comb.	55723 ± 257	4994683	60135 ± 266	4994807
$D^+ \bar{D}^0$	10098 ± 110	685784	10938 ± 114	710938
$D^0 D^-$	9713 ± 108	687883	11007 ± 113	726064
$D^+ D_s^-$	1022 ± 34	96768	725 ± 23	64425
$D_s^+ D^-$	1121 ± 36	124027	1031 ± 35	110834
$D^0 D_s^-$	2149 ± 49	296359	1631 ± 43	198031
$D_s^+ \bar{D}^0$	2520 ± 53	378137	2353 ± 52	334729
$D^+ \Lambda_c^-$	310 ± 28	25057	355 ± 28	25604
$\Lambda_c^+ D^-$	338 ± 26	49504	559 ± 32	62294
$D^0 \Lambda_c^-$	610 ± 42	76.833	683 ± 37	78606
$\Lambda_c^+ \bar{D}^0$	645 ± 42	150858	1146 ± 45	189603
$D^+ D^-$	4397 ± 74	224982	4774 ± 76	236349
$D^0 \bar{D}^0$	21944 ± 159	2104256	24398 ± 166	2190488

3.3 Study of Correlations

Contributions to the $c\bar{c}$ cross section due the leading-order perturbative QCD (α_s^2) requires the charm and anticharm quarks to be produced back-to-back in the $c\bar{c}$ center of mass. On the other hand, as the partonic center of mass is boosted in the beam direction with respect to the collision center of mass, at fixed target energies, this boost smears the longitudinal momentum correlations but preserves the transverse correlations. Therefore, leading order calculations predicts for transverse correlation variables $\Delta\phi = \pi$ rads. and $p_T^2 = 0$, but predicts small correlations in the longitudinal variable Δy .

In QCD these distributions are altered by next-to-leading order corrections (α_s^3) and non-perturbative effects (such as hadronization), as shown in references [5] and [6]. Hence, the observation of smears in the transverse and longitudinal-momentum correlations provides an indication of the importance of these before mentioned effects.

As performed in previous studies of charm-pair correlations [9–17], we compare several kinematical variables for data and Monte Carlo in order to investigate the correlations between the charm-pairs in our sample.

The kinematical variables considered for this study are:

- The azimuthal angle $\Delta\phi$ between the charm and anticharm particle momentum vectors in the plane transverse to the beam direction:

$$\Delta\phi \equiv (\text{minimum of } |\phi_{(c)} - \phi_{(\bar{c})}| \text{ and } 2\pi - |\phi_{(c)} - \phi_{(\bar{c})}|).$$

- The charm-pair squared transverse momentum:

$$p_T^2 \equiv |\vec{p}_{T,1} + \vec{p}_{T,2}|^2$$

where $p_{x(c)}$ ($p_{x(\bar{c})}$) and $p_{y(c)}$ ($p_{y(\bar{c})}$) are the charm (anticharm) transverse components of the momentum.

- The difference Δy between the charm and the anticharm rapidities:

$$\Delta\phi \equiv y_{(c)} - y_{(\bar{c})}$$

where $y \equiv \frac{1}{2} \left(\frac{E+p_z}{E-p_z} \right)$, and E and p_z are the energy and the longitudinal component of the momentum of the particles respectively.

- The invariant mass of the charm-pair.

We define the N_{prim} variable as the minimum number of particles assigned to the primary interaction vertex. This variable has a minimum value of two since it includes each charm and anticharm particle (each one counting as a single particle) in addition to charged tracks assigned to the primary vertex.

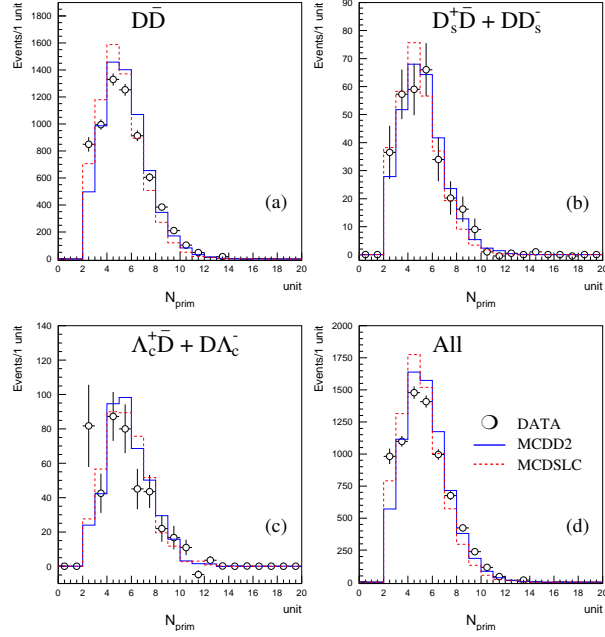


Figure 16: Number of tracks assigned to the primary vertex for background-subtracted data (open circles) and the two MC samples (MCDD2: solid blue histograms, MCDSL: dashed red histograms) normalized to the number of pairs in data.

In Fig. 16 we can see a comparison between the background-subtracted N_{prim} distributions for FOCUS data (open circles) and the two MC sets (solid and dashed histograms), for (a) $D\bar{D}$, (b) $D\bar{D}_s + DD_s^-$, (c) $D\Lambda_c^- + \Lambda_c^+ \bar{D}$ and (d) combination of all the charm-pair particles. In figures 16(a) and (c) we can observe an enhancement in the first bin ($N_{\text{prim}} = 2$) of data distributions which is not present in any of the MC distributions and could be an indication of some processes that are not considered by the PYTHIA generator⁶.

So, in order to improve comparisons between experimental data and MC model predictions we eliminate the lowest multiplicity events by requiring a $N_{\text{prim}} > 2$ cut. But ... The case for $N_{\text{prim}} = 2$ will be treated later.

In Figs. [17-28] we compare the predictions given by the two Monte Carlo sets (MCDD2: solid blue histograms, MCDSL: dashed red histograms) with the experimental background-subtracted distributions (open circles with error bars) for the kinematical variables $\Delta\phi$, p_T^2 , Δy and pair mass.

⁶It is well known for the $D\bar{D}$ sample that there is the $\psi(3770)$ state with $J=1$ (similar to the J/ψ), which is produced diffractively and is not simulated by PYTHIA.

3.3.1 Transverse Distributions for Charm-pairs

For the transverse-momentum correlation variables we observe for both the $\Delta\phi$ and the p_T^2 distributions that predictions given for the two MC sets are in fairly good agreement with the experimental data although some minor discrepancies still persist (as shown in Figs. [17-22]). On the other hand, a noteworthy enhancement is observed in the first bin of the experimental $D^0\bar{D}^0$ and $(D^0D^- + D^+\bar{D}^0)$ distributions for both variables (Figs. 18(b)-(c) and 21(b)-(c)) which is not present in any of the MC distributions, and may suggest the presence of additional production mechanisms.

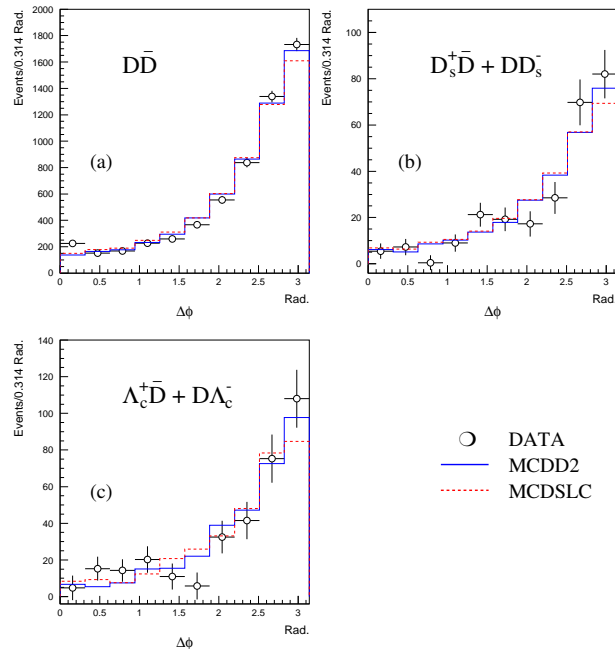


Figure 17: $D\bar{D}$, DD_s and $D\Lambda_c$ $\Delta\phi$ distributions for experimental data (open circles with error bars) compared with the two MC set predictions (MCDD2: solid blue histograms, MCDSLc: dashed red histograms).

3.3.2 Longitudinal Distributions for Charm-pairs

Similar to the transverse correlation distributions, both MC set distributions match fairly well with the experimental distributions for Δy . However, for the $D^0\bar{D}^0$ subsample the experimental data appears a little bit larger than MC predictions in the central bins of the Δy distributions (Fig. 24(b)).

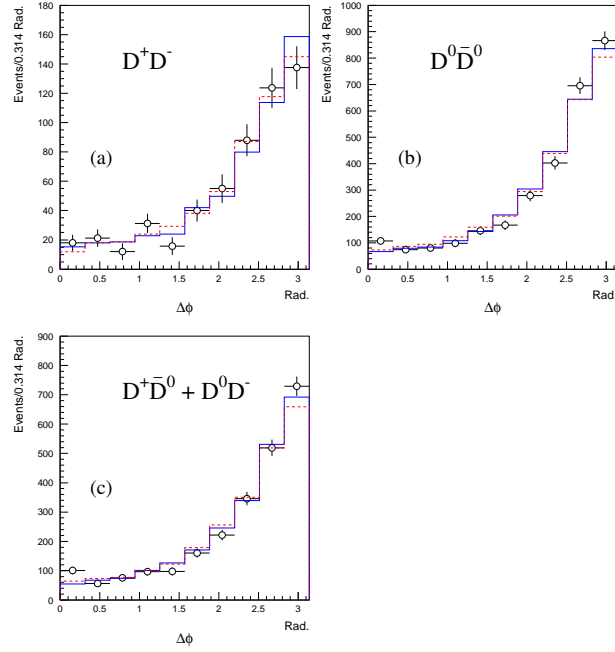


Figure 18: DD -like $\Delta\phi$ distributions for experimental data (open circles with error bars) compared with the two MC set predictions (MCDD2: solid blue histograms, MCDSL2C: dashed red histograms).

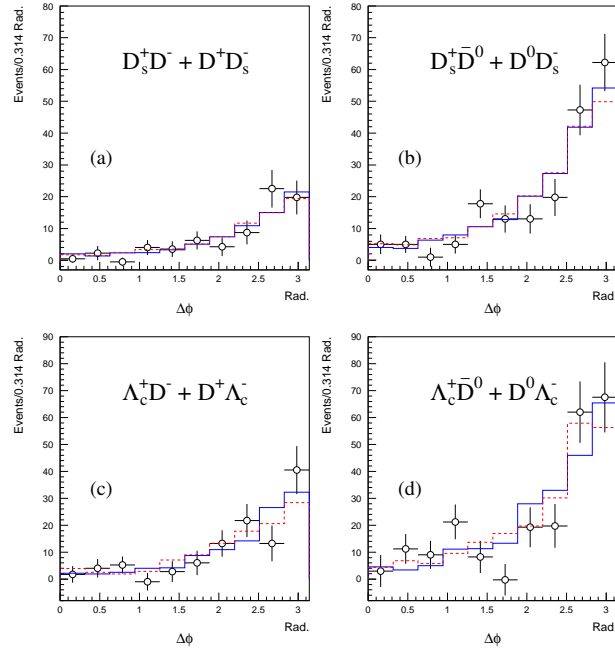


Figure 19: DD_s (top figures) and $D\Lambda_c$ -like (bottom figures) $\Delta\phi$ distributions for experimental data (open circles with error bars) compared with the two MC set predictions (MCDD2: solid blue histograms, MCDSL2C: dashed red histograms).

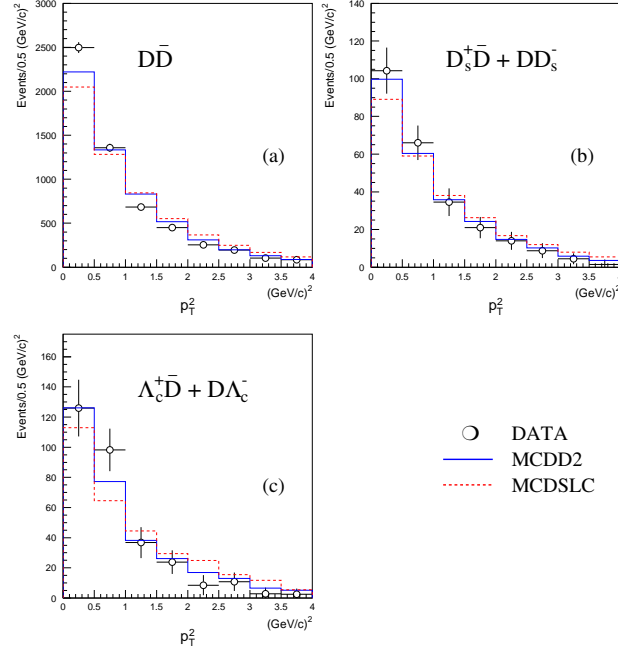


Figure 20: $D\bar{D}$, DD_s and $D\Lambda_c$ p_T^2 distributions for experimental data (open circles with error bars) compared with the two MC set predictions (MCDD2: solid blue histograms, MCDSLC: dashed red histograms).

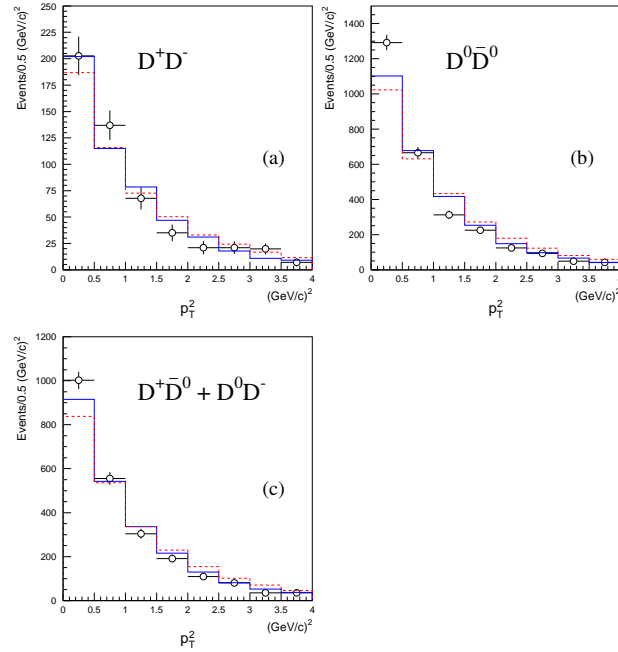


Figure 21: $D\bar{D}$ -like p_T^2 distributions for experimental data (open circles with error bars) compared with the two MC set predictions (MCDD2: solid blue histograms, MCDSLC: dashed red histograms).

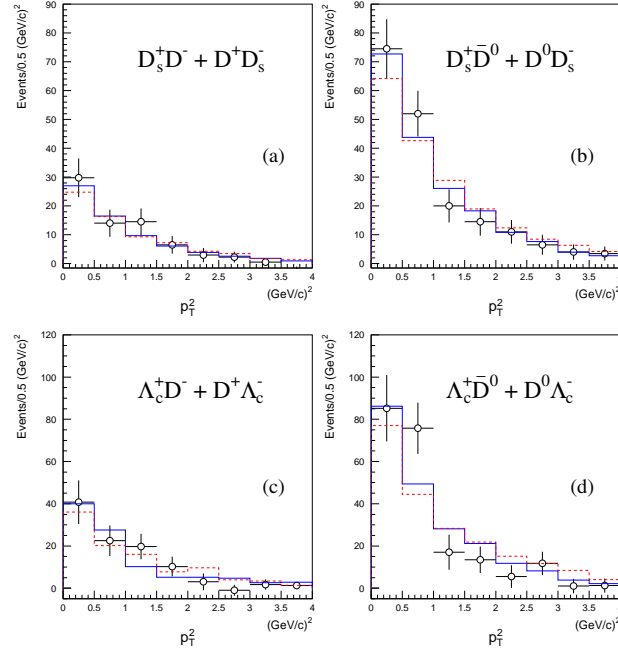


Figure 22: DD_s (top figures) and $D\Lambda_c$ -like (bottom figures) p_T^2 distributions for experimental data (open circles with error bars) compared with the two MC set predictions (MCDD2: solid blue histograms, MCDSL2: dashed red histograms).

3.3.3 Charm-pair Invariant Mass

In Figs. 26(a) and 27 we observe that the experimental charm-pair mass distributions for $D\bar{D}$ -like samples show an enhancement about $3.8 \text{ GeV}/c^2$ which is not present in any of the two MC sets mass distributions. For $D^0\bar{D}^0$ and D^+D^- mass distributions, this enhancement seems to come from the diffractive production of $\psi(3770)$ decaying into a neutral $D\bar{D}$, but for the $(D^+\bar{D}^0 + D^0D^-)$ mass distribution we don't know yet where this enhancement comes from.

For the DD_s and $D\Lambda_c$ -like samples, both MC sets predict charm-pair mass distributions compatibles with data, since the statistical errors in the data distributions are pretty large (Fig. 28).

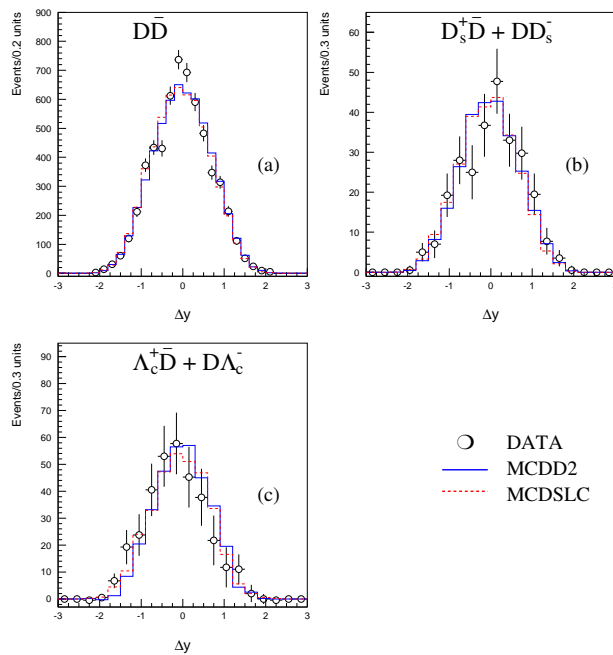


Figure 23: $D\bar{D}$, DD_s and $D\Lambda_c$ Δy distributions for experimental data (open circles with error bars) compared with the two MC set predictions (MCDD2: solid blue histograms, MCDSL: dashed red histograms).

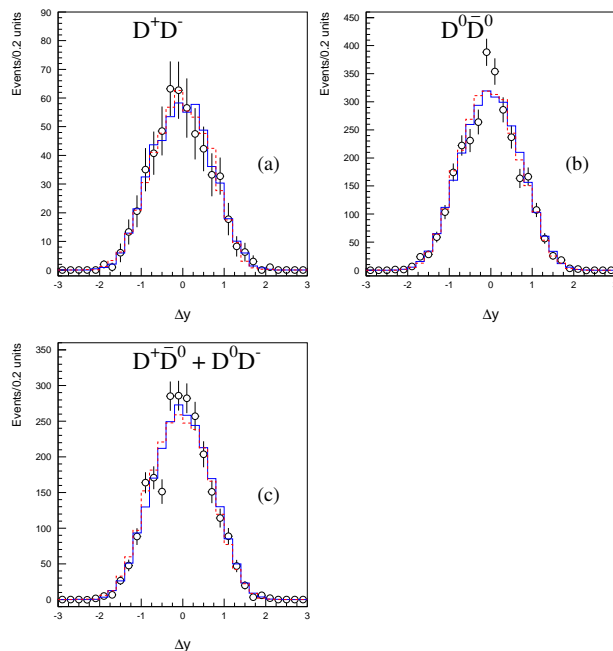


Figure 24: $D\bar{D}$ -like Δy distributions for experimental data (open circles with error bars) compared with the two MC set predictions (MCDD2: solid blue histograms, MCDSL: dashed red histograms).

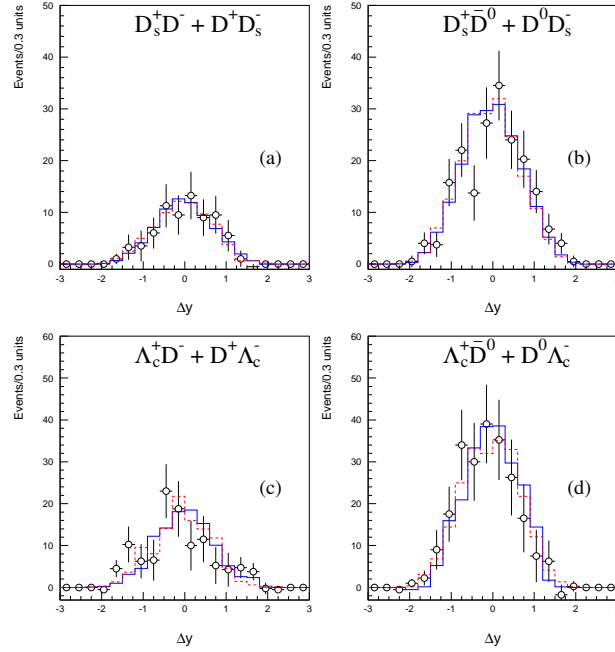


Figure 25: DD_s (top figures) and $D\Lambda_c$ -like (bottom figures) Δy distributions for experimental data (open circles with error bars) compared with the two MC set predictions (MCDD2: solid blue histograms, MCDSLc: dashed red histograms).

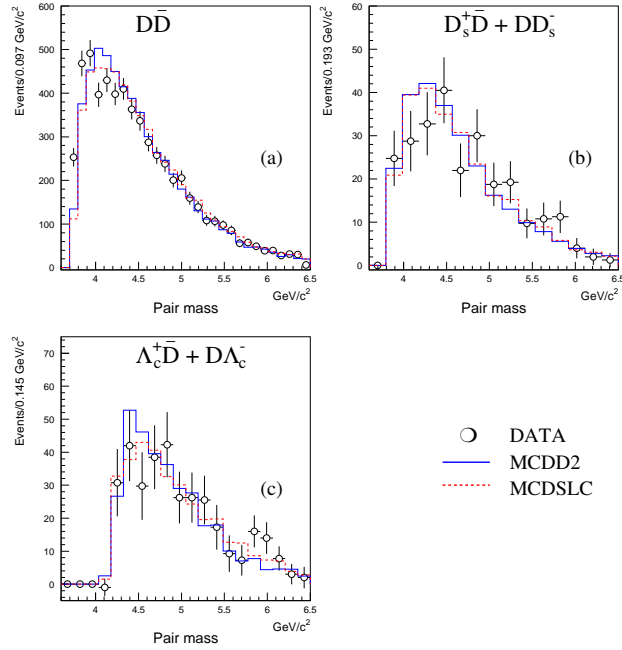


Figure 26: $D\bar{D}$, DD_s and $D\Lambda_c$ pair mass distributions for experimental data (open circles with error bars) compared with the two MC set predictions (MCDD2: solid blue histograms, MCDSLc: dashed red histograms).

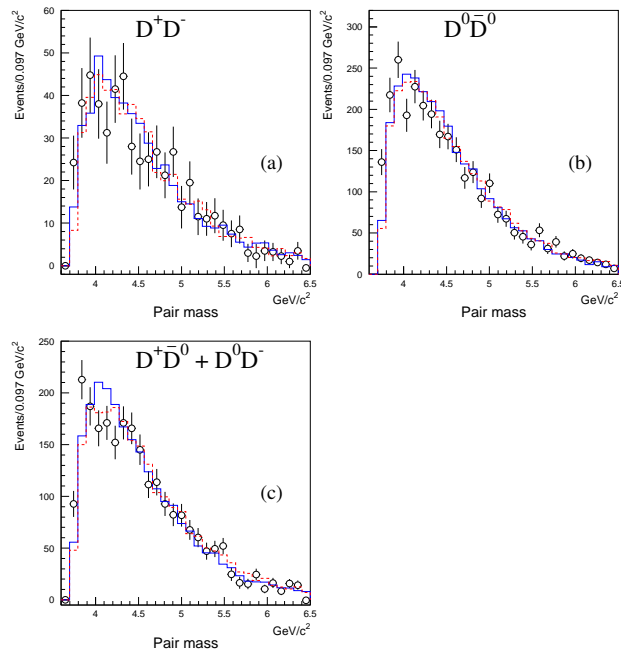


Figure 27: $D\bar{D}$ -like pair mass distributions for experimental data (open circles with error bars) compared with the two MC set predictions (MCDD2: solid blue histograms, MCDSL: dashed red histograms).

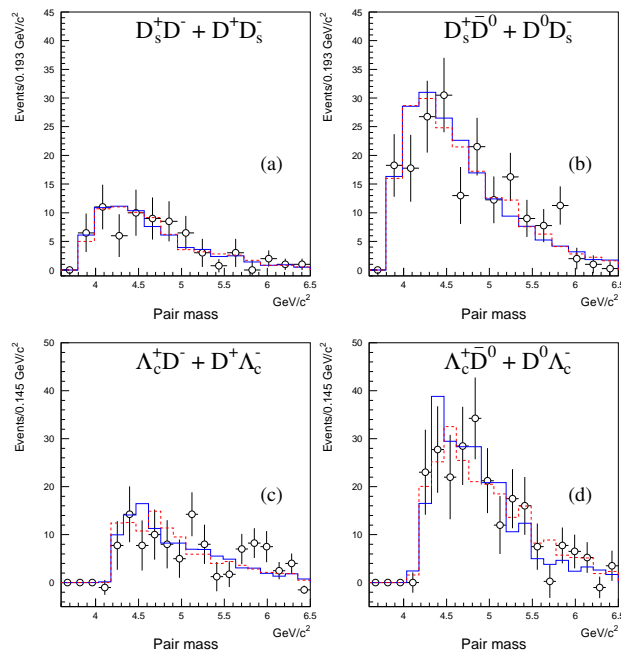


Figure 28: DD_s (top figures) and $D\Lambda_c$ -like (bottom figures) pair mass distributions for experimental data (open circles with error bars) compared with the two MC set predictions (MCDD2: solid blue histograms, MCDSL: dashed red histograms).

3.4 Charm-pair/anticharm-pair production yield ratios

The last part of the photoproduction dynamics involves the hadronization (or fragmentation) process.

After the $c\bar{c}$ pair is produced, it must dress itself into the charm hadrons we observe in experiments. But the $c\bar{c}$ pair just cannot form an isolated fragmentation string as for e^+e^- annihilation case because it would lead to a color non-singlet final state, since the $c\bar{c}$ system carries the color of the exchanged gluon. Instead, there must be some color exchange with the remnants of the target.

In the Lund fragmentation model, two independent singlet color strings are formed between the c and \bar{c} quarks and the quarks and diquarks remnants of the target nucleon: a mesonic string stretched between the \bar{c} and a target spectator quark (\mathbf{q}), and a baryonic string stretched between the c quark and the remaining target spectator diquark (\mathbf{Q}). The hadrons are created along these two independent strings in which quark-antiquark and diquark-antidiquark pairs are created along the length of the string until the available energy has been exhausted.

This scheme solves the color match problem of the photon-fusion gluon model and makes definite predictions for correlations and production ratios among the produced charmed hadrons.

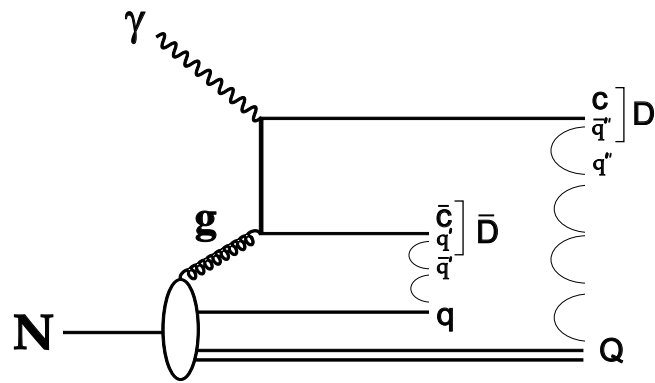
In Figs. [29-31] we show several possible combinations of the c and \bar{c} quarks with the target nucleon remnants quarks and diquarks to produce charm-pairs containing the D , D_s and Λ_c particles.

At high incident photon energies $u\bar{u}$, $d\bar{d}$ and $s\bar{s}$ quark-antiquark pairs, and $Q\bar{Q}$ diquark-antidiquark pairs are easily produced in mesonic or baryonic strings⁷, as shown in Figs. 29(a), 30(a)-(b) and 31(a)-(b). Therefore at this energy level, the production of $D^+\bar{D}^0$, DD_s^- and $D\Lambda_c^-$ charm-pairs and their corresponding antipairs (D^0D^- , $D_s^+\bar{D}$ and $\Lambda_c^+\bar{D}$) is expected to be symmetric.

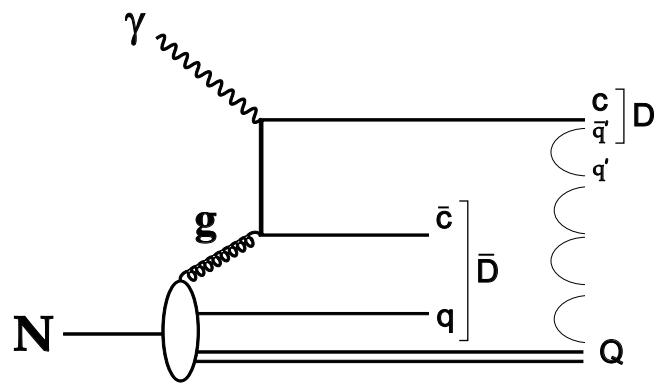
On the other hand, at low energies (below about 40 GeV), insufficient phase space is available for the production of $s\bar{s}$ quark-antiquark and $Q\bar{Q}$ diquark-antidiquark pairs but the \bar{c} antiquark (c quark) can still form a \bar{D} (Λ_c^+) through direct association with a spectator quark \mathbf{q} (diquark \mathbf{Q}) from the nucleon, as seen in Figs. 29(b), 30(c) and 31(c). Thus $D_s^+\bar{D}$ and $\Lambda_c^+\bar{D}$ charm-pairs production is expected to be favored over the production of DD_s^- and $D\Lambda_c^-$ respectively. But for $D\bar{D}$ production, as \bar{D} can be a D^- or \bar{D}^0 we expect a symmetric production of $D^+\bar{D}^0$ and D^0D^- even at these low energies.

In Table 10 we show the ratio between the reconstructed charm-pair yields and their corresponding anticharm-pair yields ($Y_{pair}/Y_{antipair}$), calculated for the $D^+\bar{D}^0$, $D^+D_s^-$, $D^0D_s^-$, $D^+\Lambda_c^-$ and $D^0\Lambda_c^-$ sub-samples, and compared with predictions given by the two Monte Carlo sets. To calculate these ratios we used the yields obtained by the binned maximum likelihood method (Tables 6 and 9).

⁷ $s\bar{s}$ and $Q\bar{Q}$ in less proportion than the other quark-antiquark pairs, in agreement with their available phase space.

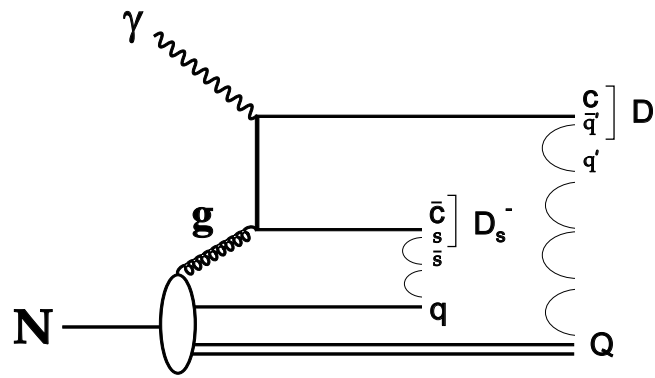


(a)

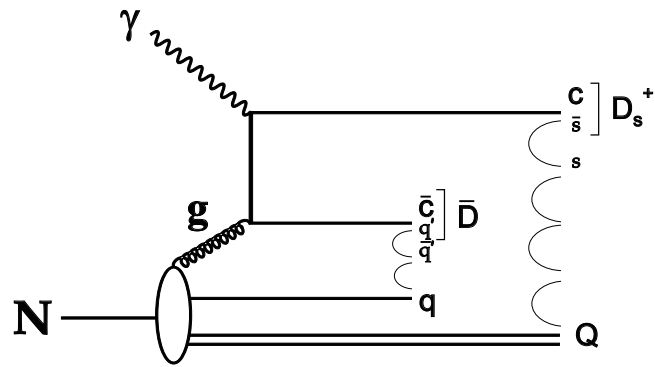


(b)

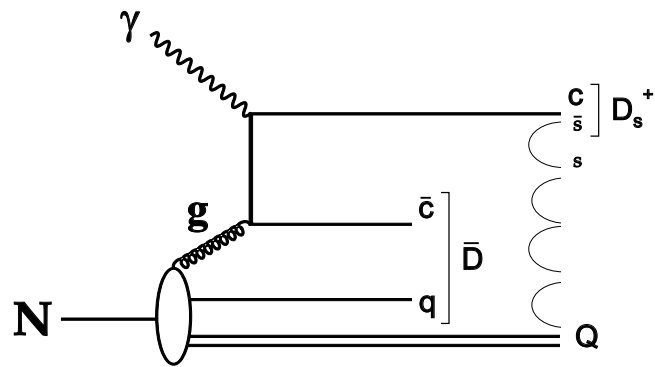
Figure 29: $D\bar{D}$ charm-pair production. (a) $\bar{D}(\bar{c}q')$ and $D(c\bar{q}')$ particles, with q' and \bar{q}' (u, d) produced in the mesonic and baryonic strings, (b) \bar{D} particle produced by $\bar{c}q$ (spectator quark) direct association.



(a)

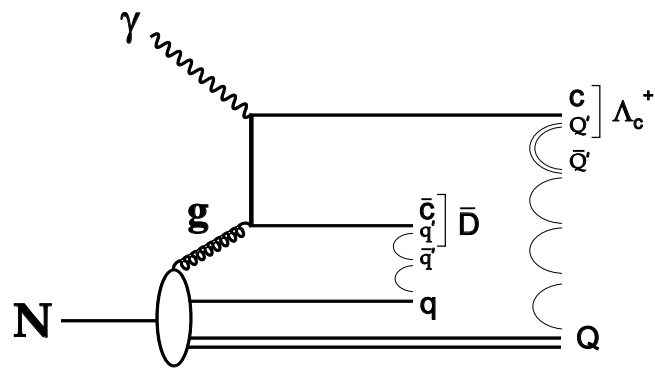


(b)

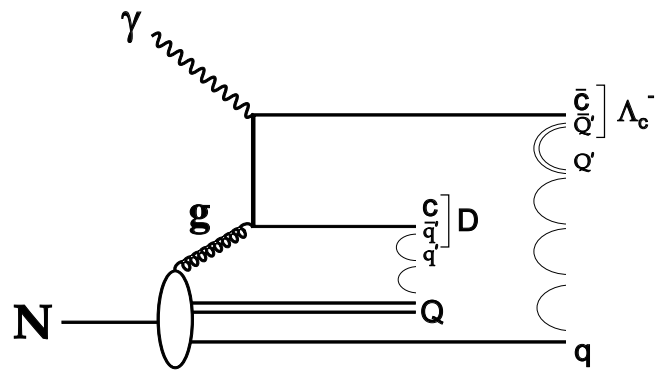


(c)

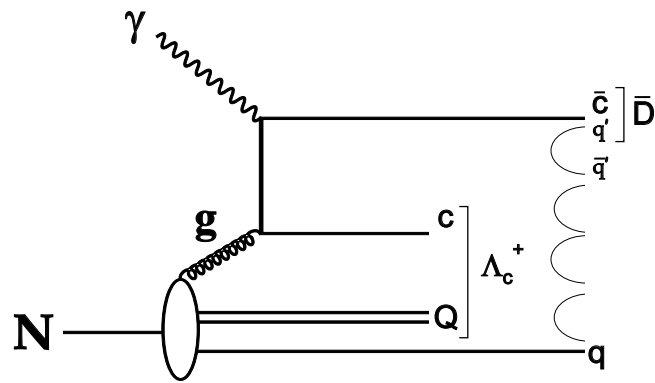
Figure 30: DD_s charm-pair production. (a) $D_s^-(\bar{c}s)$ and $D(c\bar{q}')$ particles, (b) $\bar{D}(\bar{c}q')$ and $D_s^+(c\bar{s})$ particles with q' and \bar{q}'' ($q = u, d$) produced in the mesonic and baryonic strings, (b) \bar{D} particle produced by $\bar{c}q$ (spectator quark) direct association.



(a)



(b)



(c)

Figure 31: $D\Lambda_c$ charm-pair production. (a)-(b) By combination of the c and \bar{c} quarks with quarks and antiquarks ($q' = u, d, s$) produced in the mesonic and baryonic strings, (b) \bar{D} particle produced by \bar{c} -bachelor quark direct association.

Table 10: Charm-pair/anticharm-pair yield ratios, $Y_{par}/Y_{antipar}$, for data and the two MC samples.

Ratio	Data	MCDD2	MCDSL
$\frac{Y(D^+\bar{D}^0)}{Y(D^0\bar{D}^-)}$	0.970 ± 0.055	1.040 ± 0.016	0.994 ± 0.015
$\frac{Y(D^+D_s^-)}{Y(D_s^+D^-)}$	0.837 ± 0.239	0.912 ± 0.042	0.703 ± 0.033
$\frac{Y(D^0D_s^-)}{Y(D_s^+\bar{D}^0)}$	0.681 ± 0.126	0.853 ± 0.026	0.693 ± 0.024
$\frac{Y(D^+\Lambda_c^-)}{Y(\Lambda_c^+D^-)}$	0.667 ± 0.253	0.917 ± 0.109	0.635 ± 0.062
$\frac{Y(D^0\Lambda_c^-)}{Y(\Lambda_c^+\bar{D}^0)}$	0.699 ± 0.165	0.946 ± 0.089	0.596 ± 0.040
$\frac{Y(D^+D^-)}{Y(D^0\bar{D}^0)}$	0.699 ± 0.165	0.946 ± 0.089	0.596 ± 0.040

3.5 Mini Monte Carlo Studies

A mini Monte Carlo study is usually done to check that the fit procedure produces the correct results and if the errors returned by the fit are accurate representations of the expected variability of the parameters fitted values on repetition of the experiment. It also check for biases and it can be used to assess the size and importance of any present bias.

For each charm-pair sub-sample considered in the pair/antipair ratio calculation we generate randomly 1000 bi-dimensional normalized invariant mass distributions according to the Eq. 8 and their corresponding estimated data fit parameter values (P1-P12). In order to get the number of charm-pairs for each mini Monte Carlo bi-dimensional mass distribution we use the same fit routine we applied over the data. With the yields we get, we plot a "pull" distribution⁸ for each charm-pair sub-sample, as shown in Figs. [32-36].

The pull distribution is easy to interpret if the errors are gaussian: if the parameter estimate is unbiased and the error from the fitter is accurate, then the pull distribution should be a gaussian centered at zero with width 1. In Table 11 we show a summary of the means (μ) and widths (σ) obtained from the fit of the pull distributions.

With this method we assessed some bias in the number of charm-pair events for the sub-samples $D^+\bar{D}^0$ (-5.5 ± 2.1), $D^+\Lambda_c^-$ (1.2 ± 0.3) and $\Lambda_c^+D^-$ (2.6 ± 0.8), and an underestimation of the statistical error for the sub-sample D_sD^- (3 events). Consequently the biases were subtracted for the corresponding charm-pairs and the

⁸The pull distribution is defined as:

$$pull(\alpha) = (\alpha_{mMC} - \alpha_t)/\sigma_\alpha$$

where α_t is the "true" estimated parameter value obtained from the data fit, α_{mMC} and σ_α are the estimated parameter values and their corresponding errors obtained from the fit of the mini Monte Carlo mass distributions.

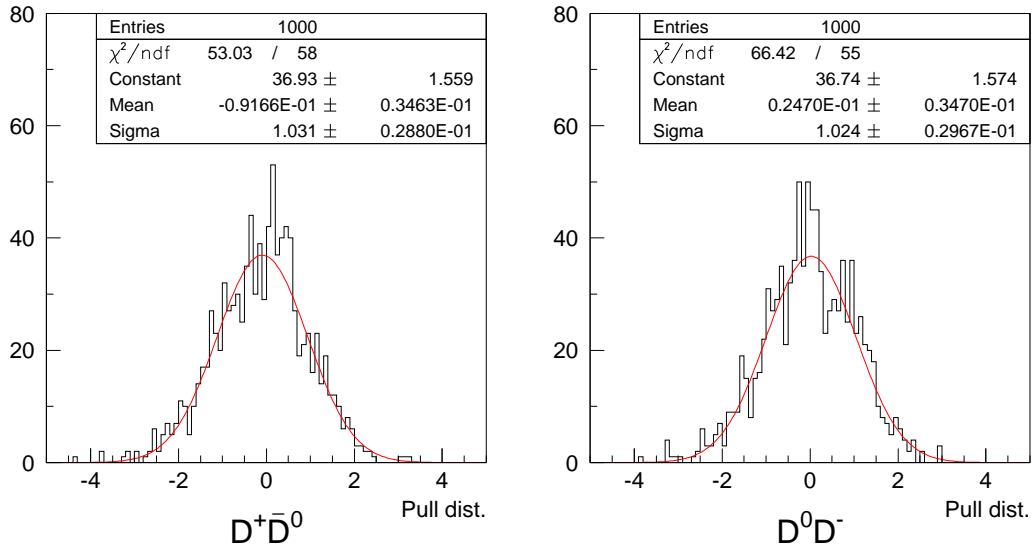


Figure 32: Pull distributions for the charm-pairs D^+D^0 and D^0D^- .

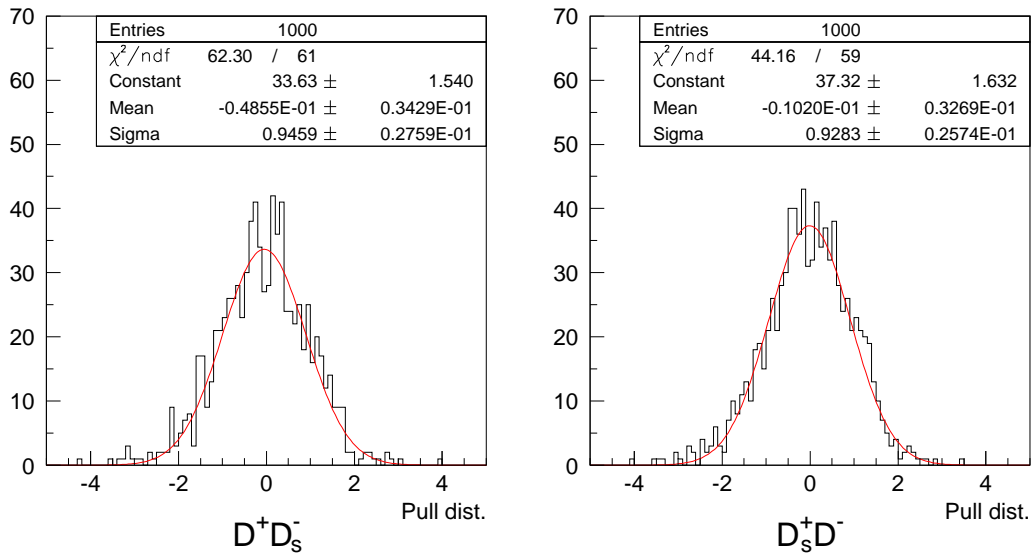


Figure 33: Pull distributions for the charm-pairs $D^+D_s^-$ and $D_s^+D^-$.

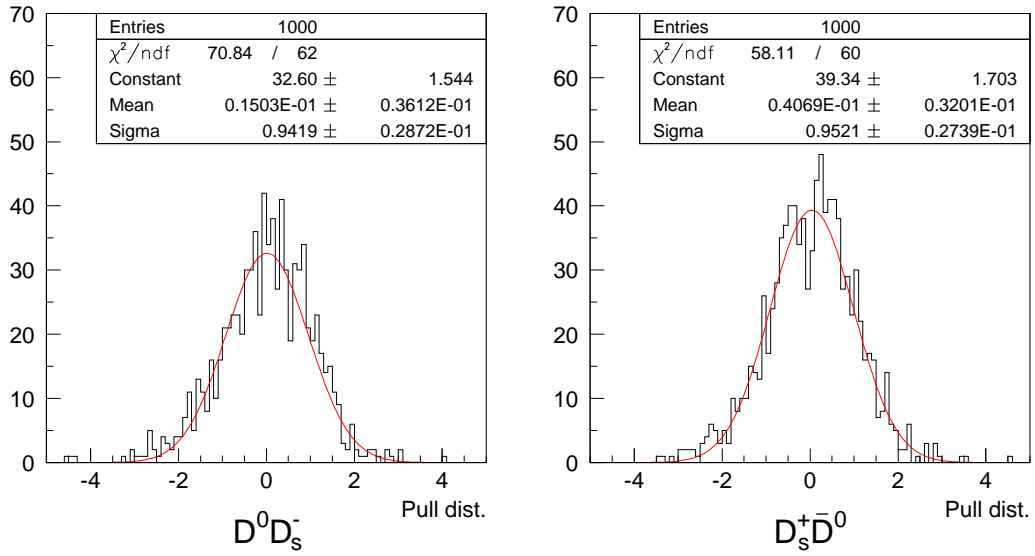


Figure 34: Pull distributions for the charm-pairs $D^0 D_s^-$ and $D_s^+ \bar{D}^0$.

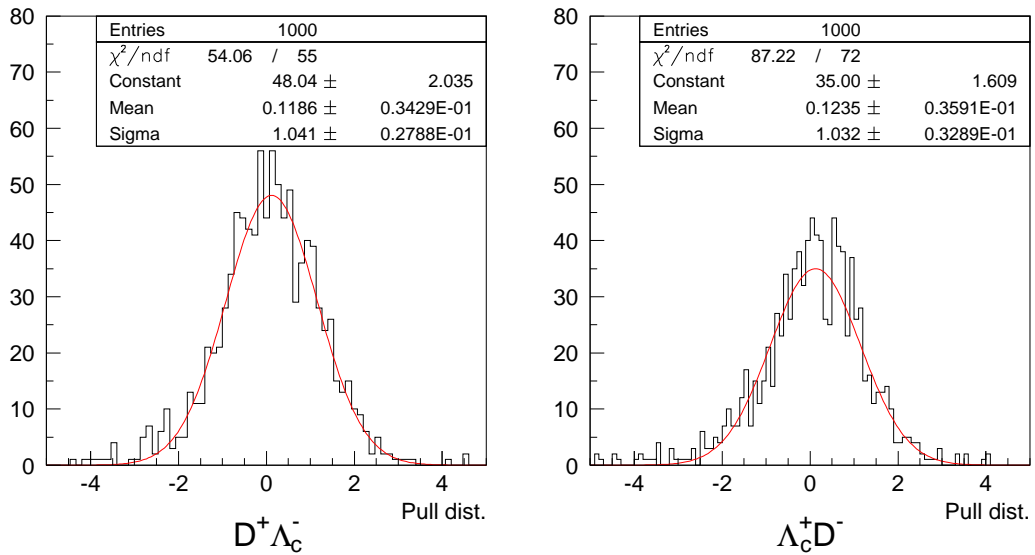


Figure 35: Pull distributions for the charm-pairs $D^+ \Lambda_c^-$ and $\Lambda_c^+ D^-$.

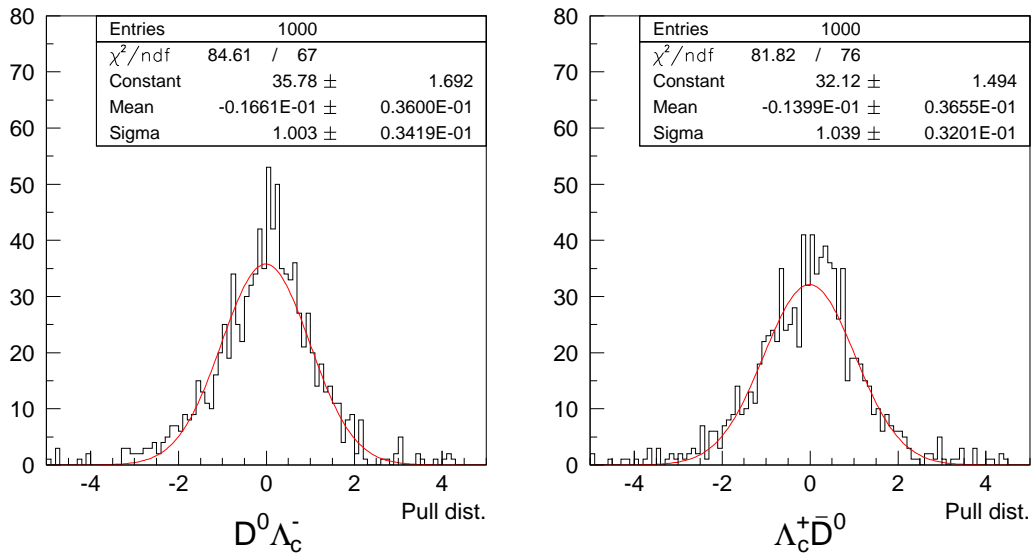


Figure 36: Pull distributions for the charm-pairs $D^0\Lambda_c^-$ and $\Lambda_c^+\bar{D}^0$.

Table 11: Summary of the means (μ) and widths (σ) obtained from the fit of the pull distributions.

Charm pair	$\mu \pm \text{err}(\mu)$	$\sigma \pm \text{err}(\sigma)$
$D^+\bar{D}^0$	-0.092 ± 0.035	1.031 ± 0.029
D^0D^-	0.025 ± 0.035	1.024 ± 0.030
$D^+D_s^-$	-0.049 ± 0.034	0.946 ± 0.028
$D_s^+D^-$	-0.010 ± 0.033	0.928 ± 0.026
$D^0D_s^-$	0.015 ± 0.036	0.942 ± 0.029
$D_s^+\bar{D}^0$	0.041 ± 0.032	0.952 ± 0.027
$D^+\Lambda_c^-$	0.119 ± 0.034	1.041 ± 0.028
$\Lambda_c^+D^-$	0.124 ± 0.036	1.032 ± 0.033
$D^0\Lambda_c^-$	-0.017 ± 0.036	1.003 ± 0.034
$\Lambda_c^+\bar{D}^0$	-0.014 ± 0.035	1.039 ± 0.032

statistical error for the sub-sample $D_s^+D^-$ was increased.

The number of events of the charm-pairs and the charm pair/antipair ratios after the mini Monte Carlo corrections are show in Table 12.

Table 12: Mini-MC corrected charm-pair yields and charm pair/antipair ratios.

Charm pair	$Y_{mMC}(corr)$	$Y_{pair}/Y_{antipair}$
D^+D^0 D^0D^-	1473 \pm 60 1510 \pm 59	0.975 \pm 0.055
$D^+D_s^-$ $D_s^+D^-$	28 \pm 7 36 \pm 11	0.778 \pm 0.307
$D^0D_s^-$ $D_s^+D^0$	47 \pm 9 69 \pm 11	0.681 \pm 0.170
$D^+\Lambda_c^-$ $\Lambda_c^+D^-$	46 \pm 12 66 \pm 21	0.697 \pm 0.287
$D^0\Lambda_c^-$ $\Lambda_c^+D^0$	127 \pm 23 176 \pm 22	0.722 \pm 0.159

3.6 Systematic checks

We perform some checks in order to assess the systematic error in the measurement of the charm pair/antipair ratios.

To do this we changed in a reasonable manner the way we get the charm-pair yields, the fitting conditions and the charm-pair momentum cut on the whole data set.

- bin25, bin30: Variation in the bin size (25×25 and 30×30 bins) of the bi-dimensional charm-pair mass distribution. ($D = 20 \times 20$ bins).
- bkgs: binned method for background subtraction ($D =$ binned maximum likelihood fit).
- p30, p40, p50: Variation in the charm-pair momentum cut ($p > 30, 40, 50$ GeV, $D = p > 0$).

With the charm-pair yields obtained from the different variations (summarized in Table 13), we calculate the different charm pair/antipair ratios (Figs. [37-39]). We suppose *a priori* that the charm pair/antipair ratios we calculate are equally likely for each couple of sub-samples, therefore the uncertainty can be estimated by the *r.m.s* of the measurements [24].

In Table 14 we show the charm pair/antipair ratios and the systematic error calculated for each sub-sample.

Finally, in Table 15 we show a comparison between the charm pair/antipair ratios we got initially and the mini Monte Carlo corrected and the systematic error added final results.

Table 13: Charm-pair yields obtained from the systematic checks.

Charm pair	Variations					
	25×25 bins	30×30 bins	Bkgs. method	P > 30	P > 40	P > 50
$Y(D^+\bar{D}^0)$	1454 ± 60	1447 ± 60	1304 ± 49	1361 ± 57	1048 ± 50	722 ± 40
$Y(D^0D^-)$	1498 ± 58	1499 ± 59	1301 ± 49	1389 ± 57	1113 ± 51	755 ± 40
$Y(D^+D_s^-)$	26 ± 7	27 ± 7	26 ± 7	23 ± 5	18 ± 6	12 ± 5
$Y(D_s^+D^-)$	38 ± 8	38 ± 8	33 ± 7	32 ± 8	23 ± 6	12 ± 5
$Y(D^0D_s^-)$	45 ± 9	47 ± 9	41 ± 9	40 ± 8	25 ± 7	11 ± 6
$Y(D_s^+\bar{D}^0)$	66 ± 11	68 ± 11	63 ± 10	59 ± 10	44 ± 9	30 ± 8
$Y(D^+\Lambda_c^-)$	50 ± 9	53 ± 10	47 ± 14	41 ± 11	28 ± 10	18 ± 7
$Y(\Lambda_c^+D^-)$	65 ± 13	66 ± 19	72 ± 15	67 ± 19	46 ± 14	34 ± 14
$Y(D^0\Lambda_c^-)$	125 ± 27	129 ± 25	136 ± 22	96 ± 24	68 ± 19	50 ± 17
$Y(\Lambda_c^+\bar{D}^0)$	194 ± 210	185 ± 21	176 ± 24	171 ± 20	105 ± 19	68 ± 12

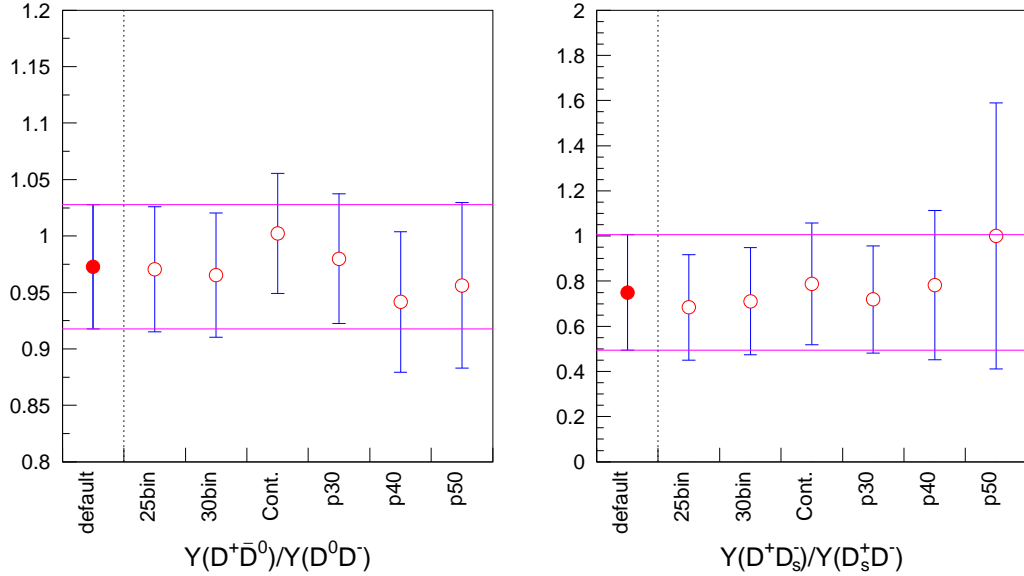


Figure 37: Systematic checks performed on the $Y(D^+\bar{D}^0)/Y(D^0D^-)$ and $Y(D^+D_s^-)/Y(D_s^+D^-)$ ratios. The first circle on the left of the plots are the values we get in this work.

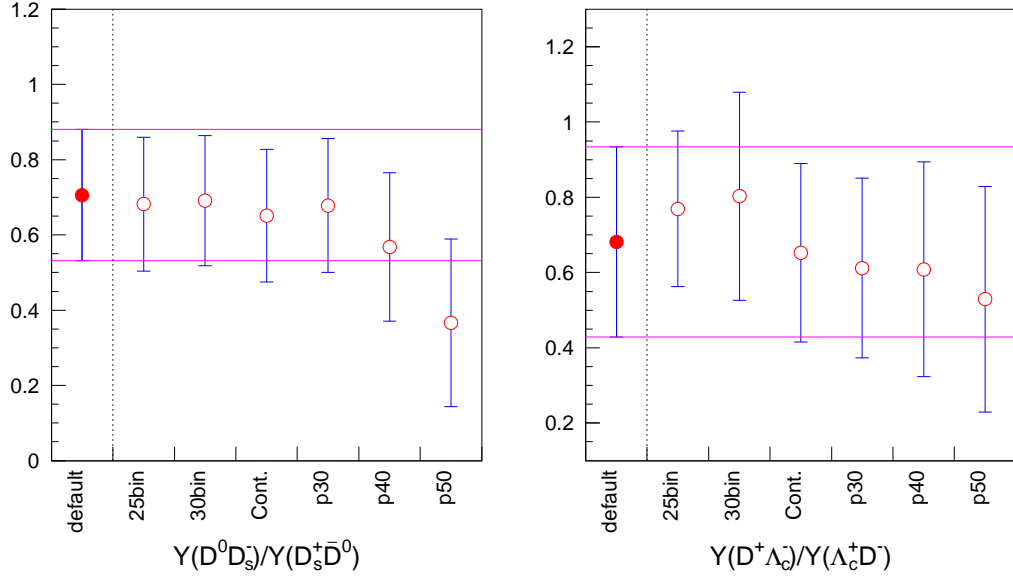


Figure 38: Systematic checks performed on the $Y(D^0 D_s^-) / Y(D_s^+ D^-)$ and $Y(D^+ \Lambda_c^-) / Y(\Lambda_c^+ D^-)$ ratios. The first circle on the left of the plots are the values we get in this work.

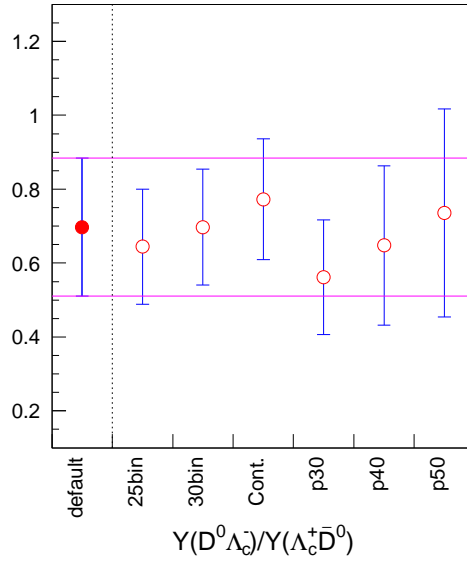


Figure 39: Systematic checks performed on the $Y(D^0 \Lambda_c^-) / Y(\Lambda_c^+ D^-)$ ratio. The first circle on the left of the plot is the value we get in this work.

Table 14: Summary of the systematic checks performed on the charm pair/antipair ratio calculations.

Ratio	25×25 bins	30×30 bins	Bkgs method	$p > 30$	$p > 40$	$p > 50$	Systematic error
$\frac{Y(D^+\bar{D}^0)}{Y(D^0D^-)}$	0.971 ± 0.047	0.965 ± 0.055	1.002 ± 0.053	0.980 ± 0.057	0.942 ± 0.062	0.956 ± 0.073	0.021
$\frac{Y(D^+D_s^-)}{Y(D_s^+D^-)}$	0.684 ± 0.234	0.711 ± 0.237	0.788 ± 0.270	0.719 ± 0.190	0.783 ± 0.331	1.000 ± 0.589	0.115
$\frac{Y(D^0D_s^-)}{Y(D_s^+\bar{D}^0)}$	0.682 ± 0.178	0.691 ± 0.173	0.651 ± 0.176	0.678 ± 0.178	0.568 ± 0.197	0.367 ± 0.223	0.126
$\frac{Y(D^+\Lambda_c^-)}{Y(\Lambda_c^+D^-)}$	0.769 ± 0.188	0.803 ± 0.285	0.653 ± 0.237	0.612 ± 0.239	0.609 ± 0.286	0.529 ± 0.300	0.104
$\frac{Y(D^0\Lambda_c^-)}{Y(\Lambda_c^+\bar{D}^0)}$	0.648 ± 0.124	0.696 ± 0.148	0.773 ± 0.163	0.561 ± 0.155	0.648 ± 0.216	0.735 ± 0.282	0.075

Table 15: Mini-MC corrected and added systematic error charm pair/antipair ratios.

Ratio	Initial Results	Final Results
$\frac{Y(D^+\bar{D}^0)}{Y(D^0\bar{D}^-)}$	0.972 ± 0.055	$0.975 \pm 0.055 \pm 0.021$
$\frac{Y(D^+D_s^-)}{Y(D_s^+D^-)}$	0.778 ± 0.256	$0.778 \pm 0.307 \pm 0.115$
$\frac{Y(D^0D_s^-)}{Y(D_s^+\bar{D}^0)}$	0.681 ± 0.170	$0.681 \pm 0.170 \pm 0.126$
$\frac{Y(D^+\Lambda_c^-)}{Y(\Lambda_c^+D^-)}$	0.681 ± 0.271	$0.697 \pm 0.287 \pm 0.104$
$\frac{Y(D^0\Lambda_c^-)}{Y(\Lambda_c^+\bar{D}^0)}$	0.722 ± 0.159	$0.722 \pm 0.159 \pm 0.075$

3.7 $N_{\text{prim}} = 2$ physics

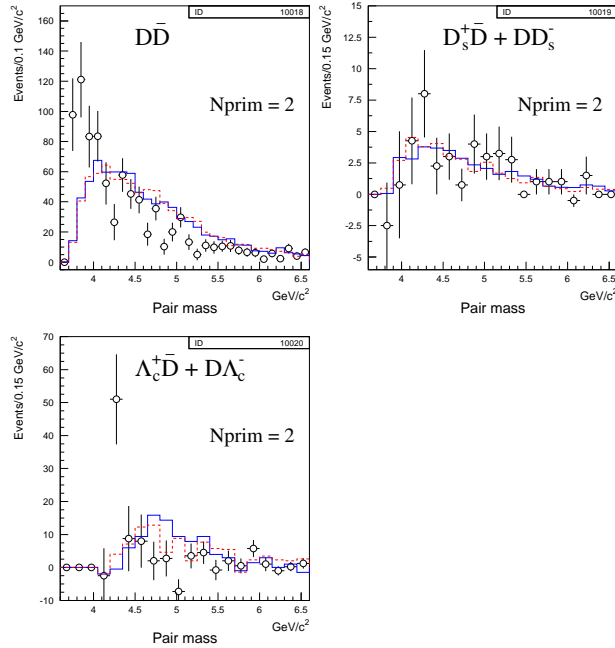


Figure 40

4 Conclusions

We have reconstructed a sample of 8423 ± 144 charm-pairs, where both final states, the charm and the anticharm, were fully reconstructed. This is the largest charm-pair sample used in an analysis of photoproduction of $c\bar{c}$ to date.

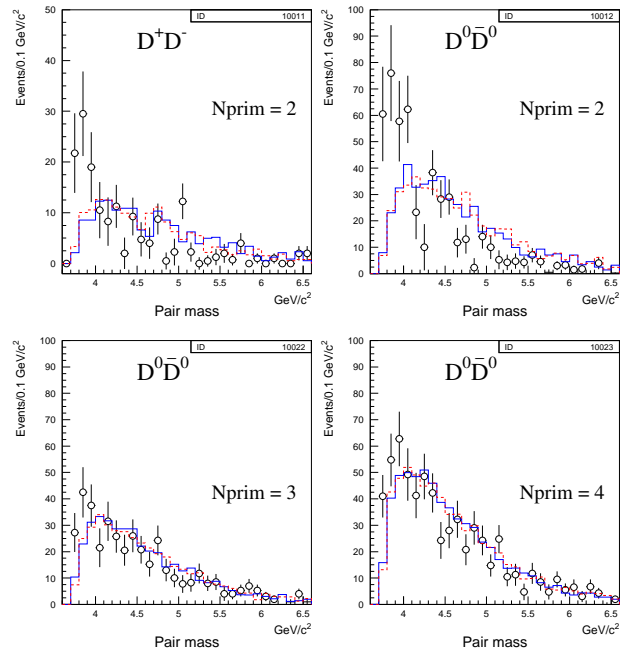


Figure 41

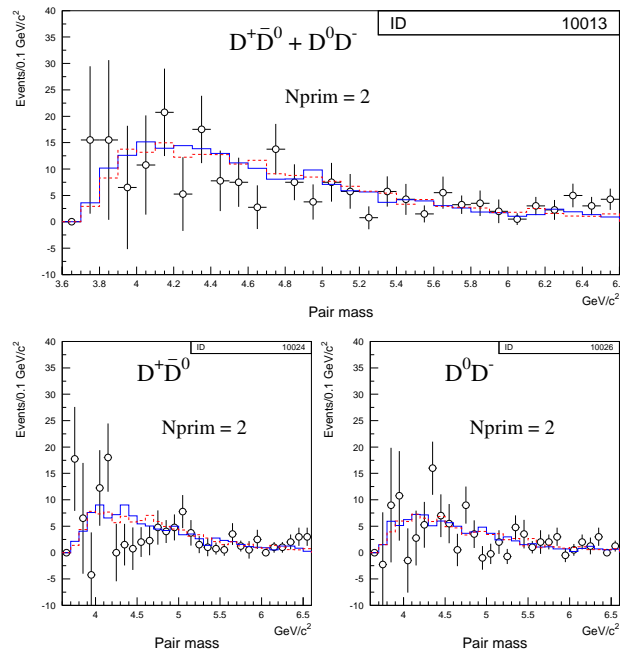


Figure 42

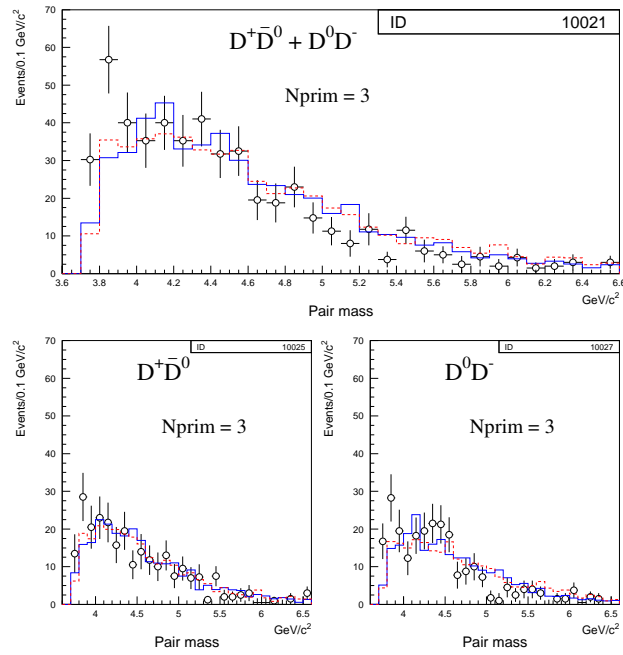


Figure 43

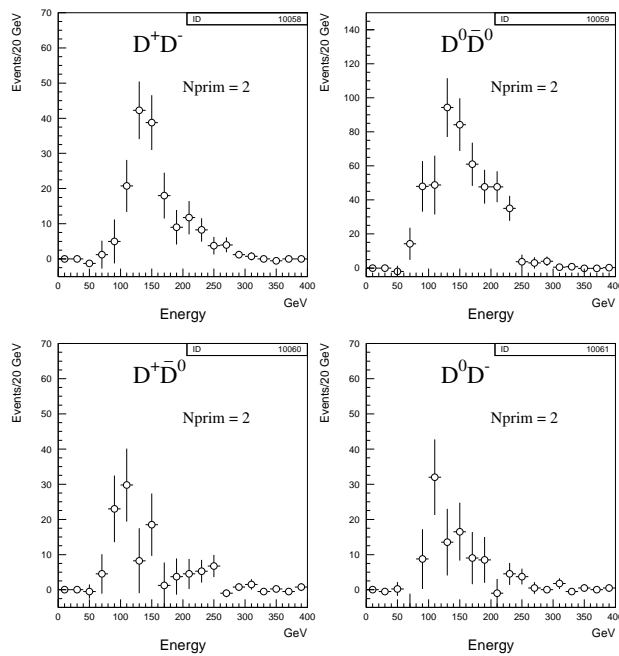


Figure 44

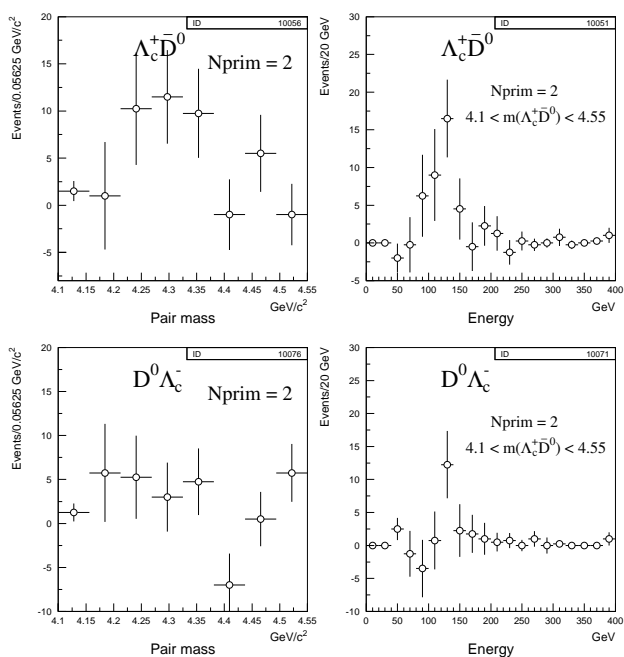


Figure 45

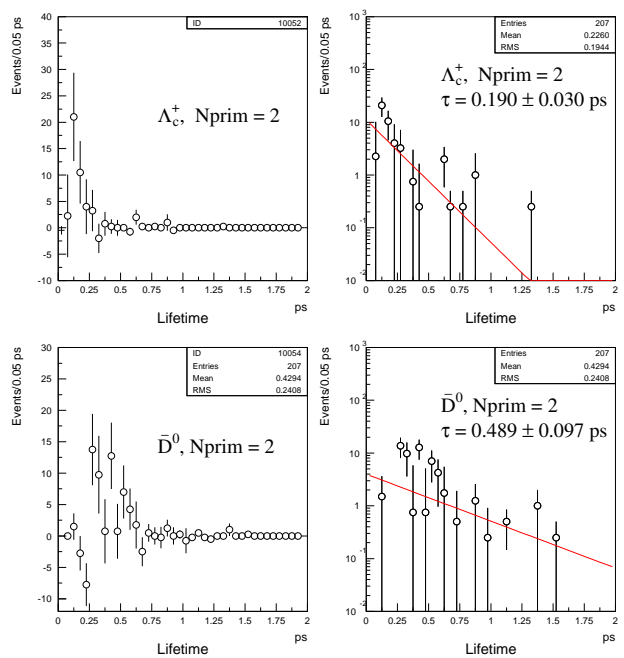


Figure 46

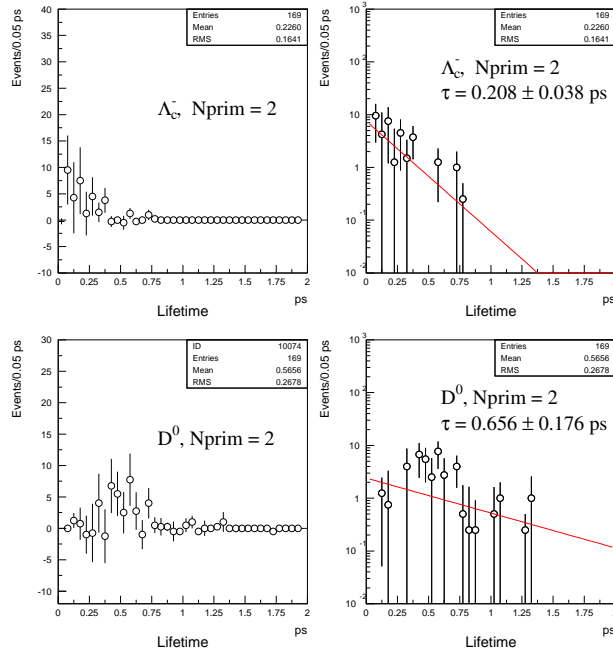


Figure 47

In addition to the reconstructed D mesons in the final states $D \rightarrow K n \pi$ ($n=1,2,3$), we also fully reconstructed the particles D_s and Λ_c in their final states $D_s \rightarrow \phi(K^+K^-)\pi$, $D_s \rightarrow \bar{K}^*(K^-\pi^+)K$ and $\Lambda_c \rightarrow pK\pi$ respectively. This gave us several advantages over the previous analysis that have used pairs of partially reconstructed D and \bar{D} mesons (eventually D_s and Λ_c), or pairs of only fully reconstructed D and \bar{D} mesons.

Because this large charm-pair sample has the final states fully reconstructed, we were able to calculate both the magnitude and direction of the charm particles momenta, which allowed us to investigate in great detail the degree of correlation between both the transverse ($\Delta\phi$, p_T^2) and longitudinal (Δy) momenta components with respect to the beam direction, as well as, the correlation in the combined mass of the charm-pairs. We were also able to calculate the pair/antipair ratios for several charm sub-samples including those containing the D_s and Λ_c particles.

We have compared all the kinematical correlation distributions and the charm pair/antipair ratios with predictions given by two Monte Carlo samples implemented with the PYTHIA event generator (v. 6.127), which make use of the three-level photon-fusion gluon process (first order of QCD) and an intrinsic transversal momentum, $\langle k_T^2 \rangle = (0.6 \text{ GeV}/c)^2$, for the partons in the target nucleon (a non-perturbative effect) to generate a couple of quarks $c\bar{c}$, as well as the Lund fragmentation model to dress the quarks into hadrons. The main difference between these two Monte Carlo sets is that one of them was tuned to favor the production of mesons D (MCDD2), and the other one to favor the D_s and Λ_c particle production (MCDSL2C).

In the comparisons of the measured and predicted charm-pair correlation distributions, we observe that the MC sample which favors the production of D mesons (MCDD2) describes the data better than the MC sample which favors the production of the particles D_s and Λ_c (MCDSL C), however some minor discrepancies persist. In the other hand, for the charm pair/antipar ratios, the two MC samples predict ratio values compatibles with data although the main ratio values predicted by the MCDSL C set are a bit closer to the data ratios than the ratios predicted by the MCDD2 set.

References

- [1] M. Luszczak, A. Szczurek, *Proceed. of DIS 2004*, Štrbské Pleso, Slovakia.
- [2] M. Luszczak, A. Szczurek, arXiv:hep-ph/0404210v1
- [3] S. Frixione, M.L. Mangano, P. Nason, G. Ridolfi, *Adv. Ser. Direct. High energy Phys.* 15 (1998) 609 [arXiv:hep-ph/9702287].
- [4] S. Frixione, M.L. Mangano, P. Nason, G. Ridolfi, *Nucl. Phys.* B 431 (1994) 453.
- [5] S. Frixione, M.L. Mangano, P. Nason, G. Ridolfi, *Nucl. Phys.* B 412 (1994) 225.
- [6] M.L. Mangano, P. Nason, G. Ridolfi, *Nucl. Phys.* B 405 (1993) 507.
- [7] M.L. Mangano, P. Nason, G. Ridolfi, *Nucl. Phys.* B 373 (1992) 295.
- [8] P. Nason, S. Dawson, R.K. Ellis, *Nucl. Phys.* B 327 (1989) 49.
- [9] E791 Collaboration, E.M. Aitala *et al.*, *EPJdirect* C4 (1999) 1.
- [10] WA92 Collaboration, M. Adamovich *et al.*, *Phys. Lett.* B 385 (1996) 487.
- [11] E653 Collaboration, K. Kodama *et al.*, *Phys. Lett.* B 263 (1991) 579.
- [12] NA32 Collaboration, S. Barlag *et al.*, *Phys. Lett.* B 257 (1991) 519; *Phys. Lett.* B 302 (1993) 112.
- [13] WA75 Collaboration, S. Aoki *et al.*, *Phys. Lett.* B 209 (1988) 113; *Prog. Theor. Phys.* 87 (1992) 1315.
- [14] NA27 Collaboration, M. Aguilar-Benitez *et al.* *Z. Phys.* C40 (1988) 321; *Phys. Lett.* B 164 (1985) 404.
- [15] FOCUS Collaboration, E. Gottschalk *et al.*, *Phys. Lett.* B 566 (2003) 51.
- [16] NA14 Collaboration, M.P. Alvarez *et al.*, *Phys. Lett.* B 278 (1992) 385.
- [17] E687 Collaboration, P.L. Frabetti *et al.*, *Phys. Lett.* B 308 (1993) 193.
- [18] PYTHIA 6.127, T. Sjöstrand *et al.*, *Comput. Phys. Commun.* 135 (2001) 238.
- [19] EZDEE Home Page, <http://www.hep.vanderbilt.edu/~sheldon/ezdee/ezdskmdoc.html>
- [20] FOCUS Collaboration, J.M. Link *et al.*, *Nucl. Inst. Meth.*, A 484 (2002) 270.
- [21] CERN Computer and Network Division, F. James, MINUIT *Reference Manual*, (1998) D506.

- [22] L.M. Jones, H.W. Wyld, *Phys. Rev. D* 17 (1978) 759.
- [23] B. Andersson, G. Gustafson and T. Sjöstrand, *Phys. Rev.* 97 (1983) 31.
- [24] FOCUS Collaboration, J.M. Link *et al.*, *Phys. Lett.*, B 555 (2003) 167.

A Monte Carlo Samples settings

A.1 MCDD2 settings

```
GENERATE      GAMMA(DO(K-,PI+),DO(K-,PI+,PI-,PI+),D+(K-,PI+,PI+),
GENERATE      LAMBDA C+(PROTON,K-,PI+),DS+(K+,K-,PI+;KKPI),
GENERATE      DOBAR(K+,PI-),DOBAR(K+,PI-,PI+,PI-),D-(K+,PI-,PI-),
GENERATE      LAMBDA C+BAR(PBAR,K+,PI-),DS-(K-,K+,PI-;KKPI))
```

```
ISEED ENV
```

```
! NUMBER ACCEPTED
```

```
MAXACC 500000
```

```
! NUMBER GENERATED
```

```
MAXGEN 499999
```

```
MIXEMBLOCK 500000
```

```
! MCS LEVEL
```

```
IMCS 71
```

```
! BREM LEVEL
```

```
BREM 1
```

```
PHOTOS 1
```

```
! NUMBER OF EVENTS TO DUMP
```

```
NDUMP 1
```

```
PILE -1
```

```
MCBEAMFILE 3
```

```
!! Production Flags
```

```
NEWPROD T
```

```
LCSTAR T
```

```
NEWPRODDSLC F
```

```
!! Spam Flags
```

```
PRINTLEVEL 1
```

```
PURGE1 T
```

```
PURGE2 T
```

```
PURGE3 T
```

```
PURGE4 T
```

```
PURGE5 T
```

```
!! Detector Flags
```

```
DOTRK T
```

```

DODRV T
DOTS T
DOOMU T
DOMU T
DOIE T
DOHC T
DOOE T
IESIMLEVEL 1
OESIMLEVEL 1
HCSIMLEVEL 1

```

```
!! Trigger Flags
```

```

DOTRIG T
TRIGLEVEL 0
EHITYPE 1

```

```
!! MIXEMUP Flags
```

```
MCRUNPERIOD -1
```

A.2 MCDSLIC settings

```

GENERATE GAMMA(DO(K-,PI+),DO(K-,PI+,PI-,PI+),D+(K-,PI+,PI+),
GENERATE LAMBDA C+(PROTON,K-,PI+),DS+(K+,K-,PI+;KKPI),
GENERATE DOBAR(K+,PI-),DOBAR(K+,PI-,PI+,PI-),D-(K+,PI-,PI-),
GENERATE LAMBDA C+BAR(PBAR,K+,PI-),DS-(K-,K+,PI-;KKPI))

```

```
ISEED ENV
```

```

! NUMBER ACCEPTED
MAXACC 500000
! NUMBER GENERATED
MAXGEN 499999
MIXEMBLOCK 500000
! MCS LEVEL
IMCS 71
! BREM LEVEL
BREM 1
PHOTOS 1

```

```

! NUMBER OF EVENTS TO DUMP
NDUMP 1

```

PILE -1
MCBEAMFILE 3

!! Production Flags

NEWPROD T
LCSTAR T
NEWPRODDSLC T

!! Spam Flags

PRINTLEVEL 1
PURGE1 T
PURGE2 T
PURGE3 T
PURGE4 T
PURGE5 T

!! Detector Flags

DOTRK T
DODRV T
DOTS T
DOOMU T
DOMU T
DOIE T
DOHC T
DOOE T
IESIMLEVEL 1
OESIMLEVEL 1
HCSIMLEVEL 1

!! Trigger Flags

DOTRIG T
TRIGLEVEL 0
EHITYPE 1

!! MIXEMUP Flags

MCRUNPERIOD -1